A Hybrid PV-FC-Diesel-Battery Efficient Schemes for Four-Wheel PMDC Electric Vehicle Drive System

Adel A. A. El-Gammal*, Adel M. Sharaf*

*Centre for Energy Studies, University of Trinidad and Tobago UTT

‡ Corresponding Author; Adel A. A. El-Gammal,Point Lisas Campus Esperanza Road, Brechin Castle, Couva. P.O. Box 957, Trinidad and Tobago, West Indies, adel.elgammal@utt.edu.tt, adel.sharaf@utt.edu.tt

Received: 09.10.2011 Accepted:28.10.2011

Abstract- the paper presents an efficient electric drive - DC scheme with an online error driven control strategies. The hybrid Photovoltaic (PV)-Fuel cell (FC)-Diesel-Battery powered four-wheel PMDC Electric Vehicle (EV) drive scheme utilizes number of dynamic self regulating control schemes. The proposed regulation schemes include Proportional plus Integral plus Derivative modified control strategies and a dynamic variable structure sliding mode control scheme which are dynamically self regulated using soft computing Particle Swarm Optimization (PSO) and Genetic Algorithm (GA) random search techniques. The PSO and GA optimal gain search and optimization techniques ensure control gains dynamical adjusting and online tuning under all operating conditions and electric vehicle nonlinearities. The Proposed tri loop dynamic error driven self tuned controllers are also used to ensure energy efficiency, control loop decoupling, AC and DC bus stabilization and efficient utilization while maintaining full speed tracking capability. The integrated scheme is fully stabilized using a novel Flexible Alternating Current Transmission System (FACTS) based green filter compensator that ensures stabilized DC bus voltage, minimal inrush current conditions, and damped load excursions.

Keywords- Diesel-driven generator, Photovoltaic PV, Fuel Cell, Backup Battery, FACTS Green Power Filter, PMDC Drives, Electric Vehicles, Dynamic Gain Adjusting, Multi Objective Optimization (MOO), Particle Swarm Optimization (PSO) and Genetic Algorithm (GA).

1. Introduction

The need to reduce fossil fuel consumption and green house gases through the use of green renewable energy sources is motivated by economic viability and environmental concerns. The shift to clean fuel technology and efficient renewable energy utilization can help reduce green house gases and reduce global warming as well as reduce heavy reliance on hydro-carbon fossil fuel sources [1-2]. The use of hybrid renewable energy sources can ensure sustainable and efficient utilization and electric AC-DC supply security [3]. EV locomotion is one of the alternative solutions for reducing fossil fuel consumption and pollutant gaseous emissions, responsible for the green house effect. However, using battery powered EV has its limitations, due to limited range battery weight size the vehicle habitability space utilization. Using hybrid AC and DC sources for EV locomotion drive allow taking advantage from their different V-I characteristics [4-5]. EV drives and propulsion systems can utilize AC and DC motor drives including new efficient Permanent Magnet DC motors [6-8]. Different classical PI, PID, fuzzy logic based, nonlinear, adaptive variable structure, model reference adaptive control, artificial neural networks, feed forward computed torque control strategies using online estimators were proposed and utilized in speed regulation and other position control applications [9-10] mostly using fixed gain control strategies. Nonlinear drive dynamics, changing mechanical inertia, friction parameters coupled with sudden load variations and drive motor parametric sensitivities due to saturation and temperature changes necessitate a flexible, fast and effective online regulation and gain adjusting/tuning methods. Several AI-related soft computing techniques, such as Genetic Algorithms (GA) and Particle Swarm Optimization (PSO) are emerging as valuable, robust, simple and effective tools for traction and industrial process automation and on-line

control adaptation [11-18]. The soft computing tools are simple flexible and reliable with strong universal property independent of gradient information and structured optimization tools. In this paper, a hybrid PV-FC-Diesel-Battery Backup scheme powering a PMDC-EV motor drive propulsion system is fully studied. The permanent magnet DC (PMDC) motor is located on each wheel of the four-wheel EV and operated in full synchronism under various control strategies. The proposed EV scheme is controlled by a number of dynamic time decoupled control strategies with optimized gains using PSO and GA random search algorithms. The PSO and GA based self regulating algorithms are utilized to track any reference speed trajectory under varying parameter and load conditions. The control system comprises four different regulators to track speed reference trajectory with minimum over/under current, inrush, ripple conditions. The proposed optimized time de-scaled and decoupled control scheme has been tested for effective dynamical speed reference trajectory tracking, efficient power utilization, limited inrush current conditions and reduced AC-DC side transients and voltage excursions.

2. Genetic Algorithm (GA)

Genetic algorithm is an optimization method inspired by Darwin's reproduction and survival of the fittest individual [11]. This algorithm looks for the fittest individual from a set of candidate solutions called population. The population is exposed to crossover, mutation and selection operators to find the fittest individual. The fitness function assesses the quality of each individual in evaluation process. The selection operator ensures the fittest individuals for the next generation. The crossover and mutation operators are used for variety of populations. The steps of genetic algorithm are depicted as follows:

1. [Start] Generate random population of n chromosomes (suitable solutions for the problem)

2. [Fitness] Evaluate the fitness f(x) of each chromosome x in the population

3. [New population] Create a new population by repeating following steps until the new population is complete

   a. [Selection] Select two parent chromosomes from a population according to their fitness (the better fitness, the bigger chance to be selected)

   b. [Crossover] With a crossover probability cross over the parents to form a new offspring (children). If no crossover was performed, offspring is an exact copy of parents.

   c. [Mutation] With a mutation probability mutate new offspring at each locus (position in chromosome).

   d. [Accepting] Place new offspring in a new population

4. [Replace] Use new generated population for a further run of algorithm

5. [Test] If the end condition is satisfied, stop, and return the best solution in current population

6. [Loop] Go to step 2

3. Particle Swarm Optimization (PSO)

Particle Swarm Optimization (PSO) is an evolutionary computation optimization technique (a search method based on a natural system) developed by Kennedy and Eberhart [12]-[15]. The system initially has a population of random selective solutions. Each potential solution is called a particle. Each particle is given a random velocity and is flown through the problem space. The particles have memory and each particle keeps track of its previous best position (called the P_{best}) and its corresponding fitness. There exist a number of Pbest for the respective particles in the swarm and the particle with greatest fitness is called the global best (G_{best}) of the swarm. The basic concept of the PSO technique lies in accelerating each particle towards its P_{best} and G_{best} locations, with a random weighted acceleration at each time step. The main steps in the particle swarm optimization algorithm and selection process are described as follows:

a Initialize a population of particles with random positions and velocities in d dimensions of the problem space and fly them.

b Evaluate the fitness of each particle in the swarm.

c For every iteration, compare each particle's fitness with its previous best fitness (Pbest) obtained. If the current value is better than Pbest, then set Pbest equal to the current value and the Pbest location equal to the current location in the d-dimensional space.

d Compare Pbest of particles with each other and update the swarm global best location with the greatest fitness (Gbest).

e Change the velocity and position of the particle According to equations (1) and (2) respectively.

$$\mathrm{V_{id}} = \omega \times V_{id} + C_1 \times rand_1 \times \left(P_{id} - X_{id}\right) + C_2 \times rand_2 \times \left(P_{gd} - X_{id}\right) \quad (1)$$

$$X_{id} = X_{id} + V_{id} \quad (2)$$

Where: Vid and Xid represent the velocity and position of the i_th particle with d dimensions, respectively. $rand_1$ and $rand_2$ are two uniform random functions, and ω is the inertia weight, which is chosen beforehand.

f Repeat steps (b) to (e) until convergence is reached based on some desired single or multiple criteria.

The PSO optimization search utilized dynamic total error minimization algorithm has many key parameters and these are described as follows: ω is called the inertia weight that controls the exploration and exploitation of the search space because it dynamically adjusts velocity. V_{max} is the

maximum allowable velocity for the particles (i.e. in the case where the velocity of the particle exceeds Vmax, then it is limited to Vmax). Thus, resolution and fitness of search depends on Vmax. If V_{max} is too high, then particles will move beyond a good solution. If V_{max} is too low, particles will be trapped in local minima. The constants C_1 and C_2 in (1) and (2), termed as cognition and social components, respectively. These are the acceleration constants which changes the velocity of a particle towards P_{best} and G_{best} (generally, somewhere between P_{best} and G_{best}). Fig. 1 shows the general flow chart of the PSO algorithm based on total error iterative minimum search. The most striking difference between PSO and the other evolutionary algorithms is that PSO chooses the path of cooperation over competition. The other optimization algorithms commonly use some form of decimation, survival of the fittest. In contrast, the PSO population is stable and individuals are not destroyed or recreated. Individuals are influenced by the best performance of their neighbors. Individuals eventually converge on optimal points in the problem domain. In addition, the PSO traditionally does not have genetic operators like crossover between individuals and mutation, and other individuals never substitute particles during the run. So, in PSO all the particles tend to converge to the best solution quickly, comparing with GA.

4. Multi-Objective Optimization

The following definitions are used in the proposed Multi-Objective Optimization (MOO) search algorithm [16-18]:

Def. 1 The general MOO problem requiring the optimization of N objectives may be formulated as follows:

Minimize

$$\vec{y} = \vec{F}(\vec{x}) = \left[\vec{f}_1(\vec{x}), \vec{f}_2(\vec{x}), \vec{f}_3(\vec{x}), \ldots, \vec{f}_N(\vec{x})\right]^T \quad (3)$$

$$\textit{subject to } g_j(\vec{x}) \le 0 \qquad j = 1,2,\ldots,M \quad (4)$$

$$\text{Where: } \vec{x}^* = \left[\vec{x}_1^*, \vec{x}_2^*, \ldots, \vec{x}_P^*\right]^T \in \Omega \quad (5)$$

$\vec{y}$ is the objective vector, the $\bar{g}_i(\bar{x})$ represents the constraints and $\vec{x}^*$ is a P-dimensional vector representing the decision variables within a parameter space Ω. The space spanned by the objective vectors is called the objective space. The subspace of the objective vectors satisfying the constraints is called the feasible space.

Def. 2 A decision vector $\vec{x}_1 \in \Omega$ is said to dominate the decision vector $\vec{x}_2 \in \Omega$ (denoted by $\vec{x}_1 \prec \vec{x}_2$), if the decision vector $\vec{x}_1$ is not worse than $\vec{x}_2$ in all objectives and strictly better than $\vec{x}_2$ in at least one objective.

Def. 3 A decision vector $\vec{x}_1 \in \Omega$ is called Pareto-optimal, if there does not exist another $\vec{x}_2 \in \Omega$ that dominates it. An objective vector is called Pareto-optimal, if the corresponding decision vector is Pareto-optimal.

Def. 4 The non-dominated set of the entire feasible search space Ω is the Pareto-optimal set. The Pareto-optimal set in the objective space is called Pareto-optimal front.

4.1. Multi-Objective Genetic Algorithm (MOGA)

The Non-Dominated Sorting Genetic Algorithm (NSGA) is a multi-objective genetic algorithm that was developed by Deb, et. al. [19]. This algorithm has been chosen over a conventional genetic algorithm for three principal reasons: (a) no need to specify a sharing parameter, (b) a strong tendency to find a diverse set of solutions along the Pareto optimal front, and (c) the ability to specify multiple objectives without the need to combine them using a weighted sum. The basic idea behind NSGA is the ranking process executed before the selection operation, as shown in Fig. 2. This process identifies non dominated solutions in the population, at each generation, to form non dominated fronts [20], after this, the selection, crossover, and mutation usual operators are performed. In the ranking procedure, the non dominated individuals in the current population are first identified. Then, these individuals are assumed to constitute the first non dominated front with a large dummy fitness value [20]. The same fitness value is assigned to all of them. In order to maintain diversity in the population, a sharing method is then applied. Afterwards, the individuals of the first front are ignored temporarily and the rest of population is processed in the same way to identify individuals for the second non dominated front. A dummy fitness value that is kept smaller than the minimum shared dummy fitness of the previous front is assigned to all individuals belonging to the new front. This process continues until the whole population is classified into non dominated fronts. Since the non dominated fronts are defined, the population is then reproduced according to the dummy fitness values.

4.2. Multi-Objective Particle Swarm Optimization (MOPSO)

In MOPSO [16-18], a set of particles are initialized in the decision space at random. For each particle i, a position x_i in the decision space and a velocity v_i are assigned. The particles change their positions and move towards the so far best-found solutions. The non-dominated solutions from the last generations are kept in the archive. The archive is an external population, in which the so far found non-dominated solutions are kept. Moving towards the optima is done in the calculations of the velocities as follows:

$$\begin{aligned} V_{id} &= \omega \times V_{id} + C_1 \times rand_1 \times \left(P_{pd} - X_{id}\right) \\ &\quad + C_2 \times rand_2 \times \left(P_{rd} - X_{id}\right) \end{aligned} \quad (6)$$

Where $P_{r,d}$, $P_{p,d}$ are randomly chosen from a single global Pareto archive, w is the inertia factor influencing the local and global abilities of the algorithm, Vi,d is the velocity of the particle i in the d_th dimension, c_1 and c_2 are weights affecting the cognitive and social factors, respectively. r_1 and r_2 are two uniform random functions in the range [0 , 1]. According to (6), each particle has to change its position X_i,d towards the position of the two guides P_r,d, P_p,d which must

be selected from the updated set of non-dominated solutions stored in the archive. The particles change their positions during generations until a termination criterion is met. Finding a relatively large set of Pareto-optimal trade-off solutions is possible by running the MOPSO for many generations. Figure 3 shows the flow chart of the Multi-Objective Particle Swarm Optimization MOPSO.

5. Sample AC-DC EV-Drive System

Figures (4-5) show the proposed all-wheel electric vehicle drive system scheme with the PV, FC sources, the diesel generator and the backup battery. The DC compensator scheme is used to ensure stable, efficient, minimal inrush operation of the hybrid renewable energy scheme. The novel PSO and GA self tuned multi regulators and coordinated controller are used for the following purposes:

1) Diesel AC generator control regulator is based on excess generation and load dynamic matching as well as stabilization of the common DC collection bus using six pulse controlled rectifier,

2) AC/DC power converter regulator to regulate the DC voltage at the Diesel engine AC bus and ensure limited inrush conditions as well as dynamic power matching to reduce current transients and improve utilization at the diesel engine interface AC-DC bus,

3) Green plug filter compensator GPFC-SPWM regulator for pulse width switching scheme to regulate the DC bus voltage and minimize inrush current transients and load excursions and/or PV and FC non linear Volt-Ampere characteristics. The GPFC device acts as a matching DC-DC interface device between the DC load dynamic characteristics and that of the hybrid main PV, FC and backup diesel generator set,

4) The permanent Magnet DC motor drive with the dynamic speed regulator that ensure speed reference tracking with minimum inrush conditions and ensure reduced voltage transients and improved energy utilization,

The unified DC-AC utilization EV-drive scheme is fully validated using the Matlab/Simulink software environment under normal conditions, DC load excursion, PMDC motor torque changes and the PV, and FC source output variations due to the inherent Volt-Ampere nonlinear relationship. Other excursion conditions in the diesel engine generator set are also introduced to assess the control system robustness, effective energy utilization and speed reference tracking.

5.1. Diesel Generator Set

From an electrical system point of view, a diesel driven AC generator can be represented as a prime mover and generator. Ideally, the prime mover has the capability to supply any power demand up to rated power at constant synchronous frequency. The synchronous generator connected to it must be able to keep the voltage constant at any load condition. The diesel engine kept the operating speed and frequency constant. When power demand fluctuates the diesel generator could vary its power output via fuel valve regulation and governor control. The synchronous generator must control its output voltage by controlling its excitation current. Thus, the diesel generating system, as an auxiliary source, must be able to control its frequency and its output voltage. The ability of the diesel generator to respond to any frequency changes is affected by the inertia of the diesel gen-set, the sensitivity of the governor, and the power capability of the diesel engine. The ability of the AC synchronous generator to control its terminal voltage can be affected by the field-winding time constant, the availability of DC excitation power to supply the field winding, and the time constant of the voltage control loop.

5.2. Photovoltaic PV

The equivalent circuit shown in Figure 6 is used to model the PV cells used in the proposed PV array [21]. This model consists of a current source, a resistor and a reverse parallel connected diode. The PVA model developed and used in Matlab/Simulink environment is based upon the circuit given in Figure 7, in which the current produced by the solar cell is equal to that produced by the current source, minus that which flows through the diode, minus that which flows through the shunt resistor:

$$I = I_L - I_D - I_{SH} \tag{7}$$

Where: I = output current, I_L = photo generated current, I_D = diode current, I_{SH} = shunt current. The current through these elements is governed by the voltage across them:

$$V_j = V + I_{RS} \tag{8}$$

Where: V_j = voltage across both diode and resistor R_{SH} (volts <http://en.wikipedia.org/wiki/Volts>), V = voltage across the output terminals (volts), I = output current (amperes), R_S = series resistance (<http://en.wikipedia.org/wiki/%CE%A9>).

The current diverted through the diode is:

$$I_D = I_o\left\{\exp\left[\frac{qV_j}{nkT}\right]-1\right\} \tag{9}$$

Where: I_0 = reverse saturation current <http://en.wikipedia.org/wiki/Saturation_current> (amperes), n = diode ideality factor (1 for an ideal diode), q = elementary charge <http://en.wikipedia.org/wiki/Elementary_charge>, k = Boltzmann's constant <http://en.wikipedia.org/wiki/Boltzmann%27s_constant>, T = absolute temperature <http://en.wikipedia.org/wiki/Absolute_temperature>.

The characteristic equation of a solar cell, which relates solar cell parameters to the output current and voltage [22]:

$$I = I_L - I_o\left\{\exp\left[\frac{q(V+IR_S)}{nkT}\right]-1\right\} - \frac{V+IR_S}{R_{SH}} \tag{10}$$

Where: R_{SH} = shunt resistance (Ω), The I-V curve of an illuminated PV cell has the shape shown in Figure 8 as the voltage across the measuring load is swept from zero to VOC, The power produced by the cell in Watts can be easily calculated along the I-V sweep by the equation P=IV. At the I_{SC} and V_{OC} points, the power will be zero and the maximum value for power will occur between the two.

5.3. Fuel Cell Battery Model

Fuel cell stacks were connected in series/parallel combination to achieve the rating desired. Fig. 8 shows a simplified diagram of the PEMFC system [23-24]. The FC model here is for a type of PEM, which uses the following electrochemical reaction:

$$H_2 + \frac{1}{2}O_2 \rightarrow H_2O + \text{Heat} + \text{Electrical Energy} \qquad (11)$$

Fig. 9 shows a simulated V - I (voltage versus current) polarization curve of a fuel cell [23-24]. As the cell current begins to increase from zero, a sudden drop of the output voltage of the fuel cell is seen. This drop of the cell voltage is due to activation voltage loss. Then, almost a linear decrease of the cell voltage is seen as the cell current increases beyond certain values, as shown in Fig. 9, which is a result of the ohmic loss. Finally, the cell voltage drops sharply to zero as the load current approaches the maximum current density that can be generated of the fuel cell. The sharp voltage drop is the effect of the concentration loss in the fuel cell. The fuel cell can be commonly modeled by simple equivalent first order circuit shown in figure 10. The open circuit voltage is modified as follows:

$$E_{oc} = N(E_n - A\ln(i_o)) \qquad (12)$$

$$\text{Where: } A = \frac{RT}{Z\alpha F} \qquad (13)$$

Where: R = 8.3145 J / (mol K), F = 96485 A s/mol, z = Number of moving electrons, E_n = Nernst voltage, which is the thermodynamics voltage of the cells and depends on the temperatures and partial pressures of reactants and products inside the stack, i_0 = Exchange current, which is the current resulting from the continual backward and forward flow of electrons from and to the electrolyte at no load. It depends also on the temperatures and partial pressures of reactants inside the stack, α = Charge transfer coefficient, which depends on the type of electrodes and catalysts used, T = Temperature of operation. The fuel cell voltage VFC is modeled as [22-23]:

$$V_{FC} = E_{oc} - V_{Activation\,Loss} - V_{Ohmic\,Loss} - V_{Concentration\,Loss} \qquad (14)$$

$$\text{Where: } V_{Activation\ Loss} = A\log\left(\frac{I_{FC} + i_n}{i_o}\right) \qquad (15)$$

$$V_{Ohmic\ Loss} = R_m\left(I_{FC} + i_n\right) \qquad (16)$$

$$V_{Concentration\ Loss} = B\log\left(1 - \frac{I_{FC} + i_n}{i_L}\right) \qquad (17)$$

Fuel cell stacks were connected in series/parallel combination to achieve the rating desired. The output of the fuel cell array was connected to a DC bus through a DC/DC converter. The DC bus voltage was kept constant via a DC bus voltage controller.

5.4. FACTS Green Plug Filter Compensator (GPFC)

The FACTS- GPFC is used to address the common concerns of inrush current conditions, voltage variations (overvoltage, under-voltage, and sustained supply interruptions), including short duration voltage variations (interruption, sags, and swells), voltage imbalance, AC-DC waveform distortion and power frequency variations [25]. The FACTS-GPFC device is used to limit the undesirable transient and inrush currents and voltage excursions.

6. Dynamic Error Driven Controller

The proposed control system comprises four regulators for the Diesel DC generator fuel throttle control, FACTS-GPFC regulator, PMDC motor drive speed tracking, and the AC/DC power converter regulator. Figures (11-14) depict the proposed multi-loop dynamic self regulating controllers based on Multi Objective Optimization search and optimization technique based on soft computing PSO and GA. The global error is the summation of the three loop individual errors including voltage stability, current limiting and synthesize dynamic power loops. Each multi loop dynamic control scheme is used to reduce a global error based on a tri-loop dynamic error summation signal and to mainly track a given speed reference trajectory loop error in addition to other supplementary motor current limiting and dynamic power loops are used as auxiliary loops to generate a dynamic global total error signal that consists of not only the main loop speed error but also the current ripple, over current limit and dynamic over load power conditions.

The global error signal is input to the self tuned controllers shown in figures (15-18). The (per-unit) three dimensional-error vector (evg ,eIg, epg) of the diesel engine controller scheme is governed by the following equations:

$$e_{vg}(k) = V_g(k)\left(\frac{1}{1+ST_g}\right)\left(\frac{1}{1+SD}\right) - V_g(k)\left(\frac{1}{1+ST_g}\right) \qquad (18)$$

$$e_{Ig}(k) = I_g(k)\left(\frac{1}{1+ST_g}\right)\left(\frac{1}{1+SD}\right) - I_g(k)\left(\frac{1}{1+ST_g}\right) \qquad (19)$$

$$e_{Pg}(k) = I_g(k)\times V_g(k)\left(\frac{1}{1+ST_g}\right)\left(\frac{1}{1+SD}\right) - I_g(k)\times V_g(k)\left(\frac{1}{1+ST_g}\right) \qquad (20)$$

The global error $e_{tg}(k)$ for the MPFC AC side scheme at a time instant:

$$e_{tg}(k) = \gamma_{vg}e_{vg}(k) + \gamma_{ig}e_{ig}(k) + \gamma_{pg}e_{pg}(k) \qquad (21)$$

In the same manner, The (per-unit) three dimensional-error vector (e_{vd} ,e_{Id}, e_{pd}) of the GPFC scheme is governed by the following equations:

$$e_{vd}(k) = V_d(k)\left(\frac{1}{1+ST_d}\right)\left(\frac{1}{1+SD}\right) - V_d(k)\left(\frac{1}{1+ST_d}\right) \quad (22)$$

$$e_{Id}(k) = I_d(k)\left(\frac{1}{1+ST_d}\right)\left(\frac{1}{1+SD}\right) - I_d(k)\left(\frac{1}{1+ST_d}\right) \quad (23)$$

$$e_{Pd}(k) = I_d(k)\times V_d(k)\left(\frac{1}{1+ST_d}\right)\left(\frac{1}{1+SD}\right) - - I_d(k)\times V_d(k)\left(\frac{1}{1+ST_d}\right) \quad (24)$$

And the global error e_{td} (k) for the DC side green plug filter compensator GPFC scheme at a time instant:

$$e_{td}(k) = \gamma_{vd}e_{vd}(k) + \gamma_{id}e_{id}(k) + \gamma_{pd}e_{pd}(k) \quad (25)$$

In addition, The (per-unit) three dimensional-error vector (e_{vR} ,e_{IR}, e_{pR}) of the three phase controlled rectifier scheme is governed by the following equations:

$$e_{vR}(k) = V_R(k)\left(\frac{1}{1+ST_R}\right)\left(\frac{1}{1+SD}\right) - V_R(k)\left(\frac{1}{1+ST_R}\right) \quad (26)$$

$$e_{IR}(k) = I_R(k)\left(\frac{1}{1+ST_R}\right)\left(\frac{1}{1+SD}\right) - I_R(k)\left(\frac{1}{1+ST_R}\right) \quad (27)$$

$$e_{PR}(k) = I_R(k)\times V_R(k)\left(\frac{1}{1+ST_R}\right)\left(\frac{1}{1+SD}\right) - - I_R(k)\times V_R(k)\left(\frac{1}{1+ST_R}\right) \quad (28)$$

The global error e_{tR} (k) for the three phase controlled converter rectifier scheme at a time instant:

$$e_{tR}(k) = \gamma_{vR}e_{vR}(k) + \gamma_{iR}e_{iR}(k) + \gamma_{pR}e_{pR}(k) \quad (29)$$

Finally, the (per-unit) three dimensional-error vector (ewm,eIm, epm) of the PMDC motor scheme is governed by the following equations:

$$e_{\omega m}(k) = \omega_m(k)\left(\frac{1}{1+ST_m}\right)\left(\frac{1}{1+SD}\right) - \omega_m(k)\left(\frac{1}{1+ST_m}\right) \quad (30)$$

$$e_{\mathrm{Im}}(k) = I_m(k)\left(\frac{1}{1+ST_m}\right)\left(\frac{1}{1+SD}\right) - I_m(k)\left(\frac{1}{1+ST_m}\right) \quad (31)$$

$$e_{Pm}(k) = I_m(k)\times \omega_m(k)\left(\frac{1}{1+ST_m}\right)\left(\frac{1}{1+SD}\right) - - I_m(k)\times \omega_m(k)\left(\frac{1}{1+ST_m}\right) \quad (32)$$

And the global error e_{tm} (k) for the MPFC scheme at a time instant:

$$e_{tm}(k) = \gamma_{\omega m}e_{\omega m}(k) + \gamma_{im}e_{im}(k) + \gamma_{pm}e_{pm}(k) \quad (33)$$

A number of conflicting objective functions are selected to optimize using the PSO algorithm. These functions are defined by the following:

$$J_1 = Minimize\left\{\left|e_{tg}\right|,\left|e_{tR}\right|,\left|e_{td}\right|,\left|e_{tm}\right|\right\} \quad (34)$$

$$J_2 = Steady\ State\ Error = \left|e_{\omega}(k)\right| = \left|\omega_{ref}(k) - \omega_m(k)\right| \quad (35)$$

$$J_3 = Settling\ Time \quad (36)$$

$$J_4 = Maximum\ Over\ Shoot \quad (37)$$

$$J_5 = Rise\ Time \quad (38)$$

In general, to solve this complex optimality search problem, there are two possible optimization techniques based on Particle Swarm Optimization (PSO): Single aggregate selected Objective Optimization SOO, which is explained and Multi Objective Optimization MOO. The main procedure of the SOO is based on selecting a single aggregate objective function with weighted single objective parameters scaled by a number of weighting factors. The objective function is optimized (either minimized or maximized) using either Genetic Algorithm GA or Particle Swarm Optimization search algorithm (PSO) methods to obtain a single global or near optimal solution. On the other hand, the main objective of the Multi-Objective (MO) problem is finding the set of acceptable (trade-off) Optimal Solutions. This set of accepted solutions is called Pareto front. These acceptable trade-off multi level solutions give more ability to the user to make an informed decision by seeing a wide range of near optimal selected solutions that are feasible and acceptable from an "overall" standpoint. Single Objective Optimization (SOO) may ignore this trade-off viewpoint, which is crucial. The main advantages of the proposed MOO method are: It doesn't require a priori knowledge of the relative importance of the objective functions, and It provides a set of acceptable trade-off near optimal solutions. This set is called Pareto front or optimality trade-off surfaces. Both SOO and MOO searching algorithms are tested, validated and compared.

The random search dynamic error driven algorithm regulates the controllers' gains using PSO and GA to minimize the system total error, the settling time, the rising time, and the maximum overshoot. The dynamic Tri Loop Error Driven controller is a novel advanced regulation concept that operates as an adaptive dynamic type multi-purpose controller capable of handling sudden parametric changes, load and/or DC source excursions. By using the Tri Loop Error Driven controller, it is expected to have a smoother, less dynamic overshoot, fast and more robust speed controller when compared to those of classical control schemes. The proposed general PMDC Motor Drive Model with the novel Tri Loop Error Driven controller are fully validated in this paper for effective reference speed trajectory tracking under different loading conditions and parametric variations; such as temperature changes while driving a complex mechanical load with non-linear parameters and/or torque-speed characteristics.

6.1. Self Tuned Conventional PID Controller

Fundamentally, the conventional PID controller comprises three basic control actions. They are simple to implement and they provide good performance. The tuning process of the gains of PID controllers can be complex because is iterative: first, it is necessary to tune the "Proportional" mode, then the "Integral", and then add the "Derivative" mode to stabilize the overshoot, then add more "Proportional", and so on. The PID controller has the following form in the time domain as shown in figure 15:

$$u(t) = K_p e(t) + K_i \int_0^t e(t)\,dt + K_d \frac{de(t)}{dt} \quad (39)$$

Where e (t) is the selected system error, u(t) the control variable, K_p the proportional gain, K_i the integral gain, and K_d is the derivative gain. Each coefficient of the PID controller adds some special characteristics to the output response of the system. Because of this, choosing the right parameters becomes a crucial decision. In this scheme, the Tri loop Error Driven Controller is utilized with traditional PID controller. PID controller gains (K_P, K_I, K_D) are dynamically self tuned using the PSO and GA dynamic search and optimization criterion based on total error minimization, steady state error, maximum overshoot, settling time and rising time.

6.2. Self Tuned Modified PID Controller- I

In the Tuned modified PID controller- I proposed controller scheme, an optimally tuned modified PID controller for the PMDC motor drive systems is developed using the Particle Swarm optimization Technique PSO and the Genetic Algorithm GA, where the additional integral of the squared system error is implemented in this modified PID controller as shown in Fig. 16,

$$u(t) = K_p e(t) + K_i \int_0^t e(t)\,dt + K_d \frac{de(t)}{dt} + K_p K_e \left(e(t)\right)^2 \quad (40)$$

The modified PID controller gains (K_P, K_I, K_D, and Ke) are tuned using the PSO searching algorithm to minimize the selected objective functions (J_1 - J_5).

6.3. Self Tuned Modified PID Controller - II

The Tuned modified PID controller-II proposed control scheme is shown in fig. 17. The resultant control voltage has the form in the time domain as:

$$u(t) = \left(K_p e(t) + K_i \int_0^t e(t)\,dt + K_d \frac{de(t)}{dt} \right) \times K_e e(t) \quad (41)$$

6.4. Self Tuned Variable Structure Sliding Mode Bang-Bang VSC/SMC/B-B Controller

In the variable structure sliding mode controller scheme, an optimally adaptive and self tuned variable structure sliding mode controller for PMDC motor drive systems using Particle Swarm optimization Technique PSO and Genetic Algorithm GA as shown in fig. 18. The slope of the sliding surface is designed as:

$$\sigma = \beta e_t + K_\alpha \frac{de_t}{dt} \quad (42)$$

With adaptive term

$$\beta = \beta_0 + \beta_1 |e_t| \quad (43)$$

Where

$$|e_t| = \sqrt{(\gamma_I e_I)^2 + (\gamma_\omega e_\omega)^2 + (\gamma_V e_V)^2 + (\gamma_p e_p)^2} \quad (44)$$

The system control voltage has the following form in the time domain [20]:the control is an on-off logic; that is: When

The PSO and GA optimization and parameters searching algorithms are implemented for tuning the gains b0, b1 and a to minimize the selected objective functions (J_1 - J_5). This test is to verify that the proposed VSC/B-B with adaptive can maintain the motor speed with nonlinear $J(\omega_m)$ and $B(\omega_m)$ even if the load changes; accordingly, the robustness can be confirmed.

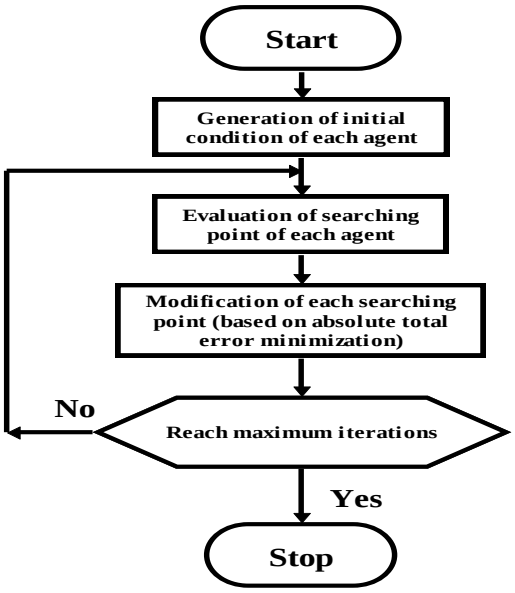

Fig. 1. Flow chart for the PSO minimizing search algorithm

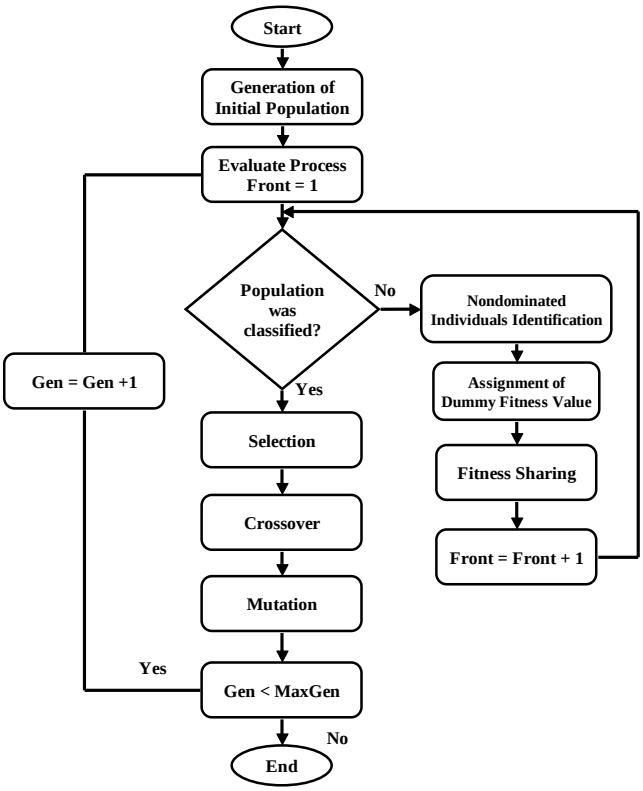

Fig. 2. Flow chart of NSGA.

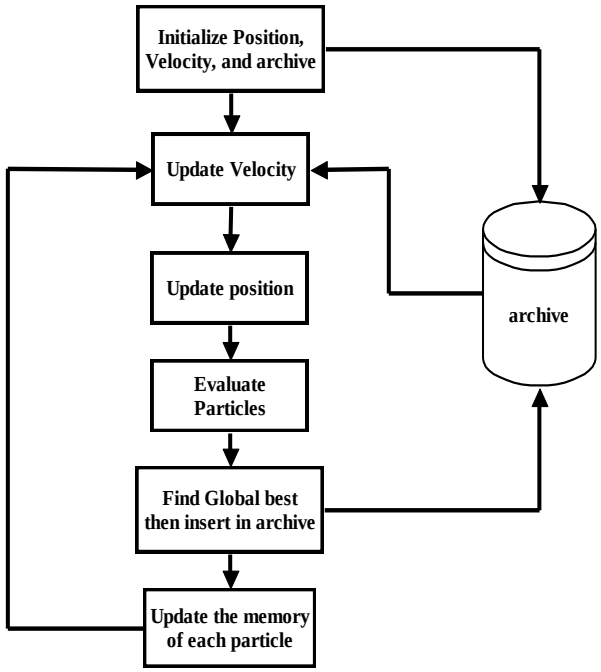

Fig. 3. Flow chart of the MOPSO optimization search algorithm

7. Digital Simulation Results

The hybrid EV-drive scheme using PV, FC, and backup diesel generation with battery backup renewable generation system performance is compared for two cases, with fixed and self tuned type controllers using either GA or PSO. The second case is to compare the performance with Artificial Neural Network ANN controller and Fuzzy Logic Controller FLC with the self tuned type controllers using either GA or PSO. All of the controllers discussed in the paper have been applied to the speed tracking control of the same EV for performance comparison. There are three different speed references. In the first speed track, the speed increases linearly and reaches the 1 PU at the end of the first five seconds, and then the reference speed remains speed constant during five seconds. At tenth second, the reference speed decreases with same slope as at the first five seconds. After fifteen second, the motor changes the direction and EV increases its speed through the reverse direction. At twentieth second, the reference speed reaches the -1 PU and remains constant speed at the end of twenty fifth second and then the reference speed decreases and becomes zero at thirtieth second. The second reference speed waveform is sinusoidal and its magnitude is 1 PU and the period is 12 seconds. The third reference track is constant speed reference starting with an exponential track. In all references, the system responses have been observed. Matlab-Simulink Software was used to design, test, and validate the effectiveness of the integrated micro grid for PMDC driven Electric Vehicle scheme using PV, FC, and backup Diesel generation with battery backup renewable generation system with the FACTS device. The digital dynamic simulation model using Matlab-Simulink software environment allows for low cost assessment and prototyping, system parameters selection and optimization of control settings. The use of PSO and GA search algorithms are used in online gain adjusting to minimize controller absolute value of total error. This is required before full scale prototyping which is both expensive and time consuming. The effectiveness of dynamic simulators brings on detailed sub-models selections and tested sub-models Matlab library of power system components already tested and validated.

The common DC bus voltage reference is set at 1 PU. Digital simulations are obtained with sampling interval Ts = 20μs. Dynamic responses obtained with GA are compared with ones resulting from the PSO for the proposed self tuned controllers. The dynamic simulation conditions are identical for all tuned controllers. To compare the global performances of all controllers, the Normalised Mean Square Error (NMSE) deviations between output plant variables and desired values, and is defined as:

$$NMSE_{V_{DC-bus}} = \frac{\sum \left(V_{DC-bus} - V_{DC-bus-ref}\right)^2}{\sum \left(V_{DC-bus-ref}\right)^2} \quad (45)$$

$$NMSE_{\omega_m} = \frac{\sum \left(\omega_m - \omega_{m-ref}\right)^2}{\sum \left(\omega_{m-ref}\right)^2} \quad (46)$$

The digital simulation results validated the effectiveness of both GA and PSO based tuned controllers in providing effective speed tracking minimal steady-state errors. Transients are also damped with minimal overshoot, settling time, and fall time. The GA and PSO based self tuned controllers are more effective and dynamically advantageous in comparison with fixed type controllers (tables 1-4), the Artificial Neural Network ANN controller (table 5) and the Fuzzy Logic Controller FLC (table 6). The self regulation is based on minimal value of absolute total/global error of each

regulator. The control system comprises the three dynamic multi loop error driven regulator is coordinated to minimize the selected objective functions. SOO obtains a single global or near optimal solution based on a single weighted objective function. The weighted single objective function combines several objective functions using specified or selected weighting factors as follows:

$$\text{weighted objective function} = = \alpha_1 J_1 + \alpha_2 J_2 + \alpha_3 J_3 + \alpha_4 J_4 + \alpha_5 J_5 \quad (47)$$

Where $\alpha_1 = 0.20$, $\alpha_2 = 0.20$, $\alpha_3 = 0.20$, $\alpha_4 = 0.20$, $\alpha_5 = 0.20$ are selected weighting factors. J_1, J_2, J_3, J_4, J_5 are the selected objective functions. On the other hand, the MO finds the set of acceptable (trade-off) Optimal Solutions. This set of accepted solutions is called Pareto front. These acceptable trade-off multi level solutions give more ability to the user to make an informed decision by seeing a wide range of near optimal selected solutions.

7.1. Self tuned classical PID controller:

Table 7 shows the DC bus dynamic behavior comparison using the GA based self tuned classical PID controller for the three selected reference tracks. In addition, table 8 shows the system dynamic behavior using the PSO based PID tuned dynamic controllers. Figures (19-24) show the effectiveness of MOPSO and MOGA search and optimized control gains in tracking the PMDC-EV motor three reference speed trajectories. Comparing the PMDC-EV dynamic response results of the two study cases, with GA and PSO tuning algorithms and traditional controllers with constant controller gains results shown in table 1, ANN controller in table 5 and FLC in table 6, it is quite apparent that the GA and PSO tuning algorithms highly improved the PMDC-EV system dynamic performance from a general power quality point of view. The GA and PSO tuning algorithms had a great impact on the system efficiency improving it from 0.873267 (constant gains controller), 0.928253 (ANN controller) and 0.937334 (FLC) to around 0.94777 (GA based tuned controller) and 0.9582 (PSO based tuned controller) which is highly desired. Moreover, The Normalized Mean Square Error (NMSE-VDC-Bus) of the DC bus voltage is reduced from 0.06263 (constant gains controller), 0.04827 (ANN controller) and 0.03022 (FLC) to around 0.007076 (GA based tuned controller) and 0.006009 (PSO based tuned controller). In addition the Normalized Mean Square Error (NMSE-wm) of the PMDC motor is reduced from 0.07681 (constant gains controller), 0.02627 (ANN controller) and 0.02016 (FLC) to around 0.008819 (GA based tuned controller) and 0.007419 (PSO based tuned controller). Maximum Transient DC Voltage Over/Under Shoot (PU) is reduced from 0.06030 (constant gains controller), 0.04186 (ANN controller) and 0.03126 (FLC) to around 0.004936 (GA based tuned controller) and 0.003582 (PSO based tuned controller). Maximum Transient DC Current - Over/Under Shoot (PU) is reduced from 0.09954 (constant gains controller), 0.07355 (ANN controller) and 0.04383 (FLC) to around 0.006094 (GA based tuned controller) and 0.005555 (PSO based tuned controller). DC bus voltage (PU) is improved from 0.8819 (constant gains controller), 0.932736 (ANN controller) and 0.94745 (FLC) to around 0.96062 (GA based tuned controller) and 0.97230 (PSO based tuned controller). DC bus current (PU) is reduced from 0.07030 (constant gains controller), 0.67464 (ANN controller) and 0.64712 (FLC) to around 0.530199 (GA based tuned controller) and 0.5425 (PSO based tuned controller). PMDCM total controller Error (etm) is reduced from 0.05513 (constant gains controller), 0.04200 (ANN controller) and 0.02154 (FLC) to around 0.008708 (GA based tuned controller) and 0.007945 (PSO based tuned controller). DC side GPFC Error (etd) is reduced from 0.04959 (constant gains controller), 0.03416 (ANN controller) and 0.02416 (FLC) to around 0.009078 (GA based tuned controller) and 0.008953 (PSO based tuned controller). The diesel engine gen set total controller Error (etg) is reduced from 0.04959 (constant gains controller), 0.04507 (ANN controller) and 0.02964 (FLC) to around 0.003974 (GA based tuned controller) and 0.002487 (PSO based tuned controller). The diesel engine converter total controller Error (etR) is reduced from 0.04249 (constant gains controller), 0.03978 (ANN controller) and 0.0260 (FLC) to around 0.006566 (GA based tuned controller) and 0.005391 (PSO based tuned controller).

7.2. Self tuned weighted modified PID controller- I:

Table 9 shows the DC bus dynamic behavior comparison using the GA based modified PID tuned dynamic controllers-I for the three selected reference tracks. In addition, table 10 shows the system dynamic behavior using the PSO based modified PID tuned dynamic controllers-I. Figures (25-30) show the effectiveness of MOPSO and MOGA search and optimized control gains in tracking the PMDC-EV motor three reference speed trajectories. Comparing the PMDC-EV dynamic response results of the two study cases, with GA and PSO tuning algorithms and traditional controllers with constant controller gains results shown in table 2, ANN controller in table 5 and FLC in table 6, it is quite apparent that the GA and PSO tuning algorithms highly improved the PMDC-EV system dynamic performance from a general power quality point of view. The GA and PSO tuning algorithms had a great impact on the system efficiency improving it from 0.891517 (constant gains controller), 0.928253 (ANN controller) and 0.937334 (FLC) to around 0.933797 (GA based tuned controller) and 0.95622 (PSO based tuned controller) which is highly desired. Moreover, The Normalized Mean Square Error (NMSE-VDC-Bus) of the DC bus voltage is reduced from 0.08323 (constant gains controller), 0.04827 (ANN controller) and 0.03022 (FLC) to around 0.009372 (GA based tuned controller) and 0.007157 (PSO based tuned controller). In addition the Normalized Mean Square Error (NMSE-wm) of the PMDC motor is reduced from 0.05022 (constant gains controller), 0.02627 (ANN controller) and 0.02016 (FLC) to around 0.007118 (GA based tuned controller) and 0.006477 (PSO based tuned controller). Maximum Transient DC Voltage Over/Under Shoot (PU) is reduced from 0.062632 (constant gains controller), 0.04186 (ANN controller) and 0.03126 (FLC) to around 0.009151 (GA based tuned controller) and 0.007736 (PSO based tuned controller). Maximum Transient DC

Current - Over/Under Shoot (PU) is reduced from 0.085243 (constant gains controller), 0.07355 (ANN controller) and 0.04383 (FLC) to around 0.008397 (GA based tuned controller) and 0.007235 (PSO based tuned controller). DC bus voltage (PU) is improved from 0.903496 (constant gains controller), 0.932736 (ANN controller) and 0.94745 (FLC) to around 0.9861 (GA based tuned controller) and 0.97350 (PSO based tuned controller). DC bus current (PU) is reduced from 0.71977 (constant gains controller), 0.67464 (ANN controller) and 0.64712 (FLC) to around 0.62814 (GA based tuned controller) and 0.61669 (PSO based tuned controller). PMDCM total controller Error (etm) is reduced from 0.08924 (constant gains controller), 0.04200 (ANN controller) and 0.02154 (FLC) to around 0.007699 (GA based tuned controller) and 0.005898 (PSO based tuned controller). DC side GPFC Error (etd) is reduced from 0.07240 (constant gains controller), 0.03416 (ANN controller) and 0.02416 (FLC) to around 0.006135 (GA based tuned controller) and 0.004256 (PSO based tuned controller). The diesel engine gen set total controller Error (etg) is reduced from 0.064996 (constant gains controller), 0.04507 (ANN controller) and 0.02964 (FLC) to around 0.006440 (GA based tuned controller) and 0.007857 (PSO based tuned controller). The diesel engine converter total controller Error (etR) is reduced from 0.053814 (constant gains controller), 0.03978 (ANN controller) and 0.0260 (FLC) to around 0.007476 (GA based tuned controller) and 0.007545 (PSO based tuned controller).

7.3. Self tuned weighted modified PID controller - II:

Table 11 shows the DC bus dynamic behavior comparison using the GA based modified PID tuned dynamic controllers-II for the three selected reference tracks. In addition, table 12 shows the system dynamic behavior using the PSO based PID tuned dynamic controllers. Figures (31-36) show the effectiveness of MOPSO and MOGA search and optimized control gains in tracking the PMDC-EV motor three reference speed trajectories. Comparing the PMDC-EV dynamic response results of the two study cases, with GA and PSO tuning algorithms and traditional controllers with constant controller gains results shown in table 3, ANN controller in table 5 and FLC in table 6, it is quite apparent that the GA and PSO tuning algorithms highly improved the PMDC-EV system dynamic performance from a general power quality point of view. The GA and PSO tuning algorithms had a great impact on the system efficiency improving it from 0.91325 (constant gains controller), 0.928253 (ANN controller) and 0.937334 (FLC) to around 0.94371 (GA based tuned controller) and 0.953824 (PSO based tuned controller) which is highly desired. Moreover, The Normalized Mean Square Error (NMSE-VDC-Bus) of the DC bus voltage is reduced from 0.06109 (constant gains controller), 0.04827 (ANN controller) and 0.03022 (FLC) to around 0.005516 (GA based tuned controller) and 0.006396 (PSO based tuned controller). In addition the Normalized Mean Square Error (NMSE-wm) of the PMDC motor is reduced from 0.06130 (constant gains controller), 0.02627 (ANN controller) and 0.02016 (FLC) to around 0.006859 (GA based tuned controller) and 0.0054443 (PSO based tuned controller). Maximum Transient DC Voltage Over/Under Shoot (PU) is reduced from 0.0655 (constant gains controller), 0.04186 (ANN controller) and 0.03126 (FLC) to around 0.0054632 (GA based tuned controller) and 0.0053175 (PSO based tuned controller). Maximum Transient DC Current - Over/Under Shoot (PU) is reduced from 0.09802 (constant gains controller), 0.07355 (ANN controller) and 0.04383 (FLC) to around 0.008899 (GA based tuned controller) and 0.00753175 (PSO based tuned controller). DC bus voltage (PU) is improved from 0.91325 (constant gains controller), 0.932736 (ANN controller) and 0.94745 (FLC) to around 0.96469 (GA based tuned controller) and 0.964346 (PSO based tuned controller). DC bus current (PU) is reduced from 0.74441 (constant gains controller), 0.67464 (ANN controller) and 0.64712 (FLC) to around 0.61953 (GA based tuned controller) and 0.618023 (PSO based tuned controller). PMDCM total controller Error (etm) is reduced from 0.08187 (constant gains controller), 0.04200 (ANN controller) and 0.02154 (FLC) to around 0.0013194 (GA based tuned controller) and 0.0015124 (PSO based tuned controller). DC side GPFC Error (etd) is reduced from 0.06634 (constant gains controller), 0.03416 (ANN controller) and 0.02416 (FLC) to around 0.0052439 (GA based tuned controller) and 0.0064763 (PSO based tuned controller). The diesel engine gen set total controller Error (etg) is reduced from 0.054390 (constant gains controller), 0.04507 (ANN controller) and 0.02964 (FLC) to around 0.004942 (GA based tuned controller) and 0.005347 (PSO based tuned controller). The diesel engine converter total controller Error (etR) is reduced from 0.04346 (constant gains controller), 0.03978 (ANN controller) and 0.0260 (FLC) to around 0.0066789 (GA based tuned controller) and 0.0074459 (PSO based tuned controller).

7.4. Self tuned Variable Structure Sliding Mode Controller VSC/SMC/B-B:

Table 13 shows the DC bus dynamic behavior comparison using the GA based Self tuned Variable structure sliding mode controller for the three selected reference tracks. In addition, table 14 shows the system dynamic behavior using the PSO based PID tuned dynamic controllers. Figures (37-42) show the effectiveness of MOPSO and MOGA search and optimized control gains in tracking the PMDC-EV motor three reference speed trajectories. Comparing the PMDC-EV dynamic response results of the two study cases, with GA and PSO tuning algorithms and traditional controllers with constant controller gains results shown in table 4, ANN controller in table 5 and FLC in table 6, it is quite apparent that the GA and PSO tuning algorithms highly improved the PMDC-EV system dynamic performance from a general power quality point of view. The GA and PSO tuning algorithms had a great impact on the system efficiency improving it from 0.906631 (constant gains controller), 0.928253 (ANN controller) and 0.937334 (FLC) to around 0.948156 (GA based tuned controller) and 0.930708 (PSO based tuned controller) which is highly desired. Moreover, The Normalized Mean Square Error (NMSE-VDC-Bus) of the DC bus voltage is reduced from 0.08443 (constant gains controller), 0.04827 (ANN controller) and 0.03022 (FLC) to around 0.007304 (GA based tuned controller) and 0.005854 (PSO based tuned

controller). In addition the Normalized Mean Square Error (NMSE-wm) of the PMDC motor is reduced from 0.053548 (constant gains controller), 0.02627 (ANN controller) and 0.02016 (FLC) to around 0.0076308 (GA based tuned controller) and 0.006309 (PSO based tuned controller). Maximum Transient DC Voltage Over/Under Shoot (PU) is reduced from 0.054604 (constant gains controller), 0.04186 (ANN controller) and 0.03126 (FLC) to around 0.009302 (GA based tuned controller) and 0.007259 (PSO based tuned controller). Maximum Transient DC Current - Over/Under Shoot (PU) is reduced from 0.087336 (constant gains controller), 0.07355 (ANN controller) and 0.04383 (FLC) to around 0.00292 (GA based tuned controller) and 0.005987 (PSO based tuned controller). DC bus voltage (PU) is improved from 0.917020 (constant gains controller), 0.932736 (ANN controller) and 0.94745 (FLC) to around 0.97417 (GA based tuned controller) and 0.974602 (PSO based tuned controller). DC bus current (PU) is reduced from 0.769594 (constant gains controller), 0.67464 (ANN controller) and 0.64712 (FLC) to around 0.614695 (GA based tuned controller) and 0.607674 (PSO based tuned controller). PMDCM total controller Error (etm) is reduced from 0.095145 (constant gains controller), 0.04200 (ANN controller) and 0.02154 (FLC) to around 0.009167 (GA based tuned controller) and 0.0048638 (PSO based tuned controller). DC side GPFC Error (etd) is reduced from 0.70746 (constant gains controller), 0.03416 (ANN controller) and 0.02416 (FLC) to around 0.004618 (GA based tuned controller) and 0.0074294 (PSO based tuned controller). The diesel engine gen set total controller Error (etg) is reduced from 0.067513 (constant gains controller), 0.04507 (ANN controller) and 0.02964 (FLC) to around 0.005121 (GA based tuned controller) and 0.007013 (PSO based tuned controller). The diesel engine converter total controller Error (etR) is reduced from 0.086233 (constant gains controller), 0.03978 (ANN controller) and 0.0260 (FLC) to around 0.003265 (GA based tuned controller) and 0.0053836 (PSO based tuned controller).

8. Conclusion

The paper validated a novel hybrid AC-DC EV drive scheme with self regulating soft computing AI based PSO and GA search algorithms are used in gain tuning. The EV PMDC-drive system is powered by a hybrid integrated renewable energy (PV-FC-Diesel-Battery) system. A number of weighted modified PID and variable structure control strategies are fully validated for effective speed reference tracking, minimal overshoot and steady state error. The proposed control strategies utilize multi-loop error driven time-discalced decoupled regulation loops with dynamic tunable gains and settings dynamically optimized and adjusted using multi-objective PSO/GA random search and optimization algorithm. The hybrid EV-PMDC drive system is fully stabilized using the FACTS-GPFC located at the common DC-bus. The FACTS-GPFC device ensures stabilized DC bus voltage, minimal overvoltage transients and limited inrush current conditions. The near optimal dynamic iterative search and optimization results show the effectiveness of the Multi Objective Particle Swarm Optimization approach MOPSO and Genetic Algorithm MOGA to effectively control the power transfer and efficient energy utilization from all renewable energy sources to the PMDC motor drives while ensuring minimum inrush current and ripple conditions. The hybrid AC-DC EV scheme was simulated using Matlab-Simulink software environment. The hybrid scheme using other novel AC and DC side FACTS devices and coordinated multi-regulation control strategies is being extended to hybrid renewable green energy (Wind, PV, FC, Gas Turbine, Micro-Hydro, …) for village/Island electricity and smart grid Vehicle to Grid (V2G) Applications.

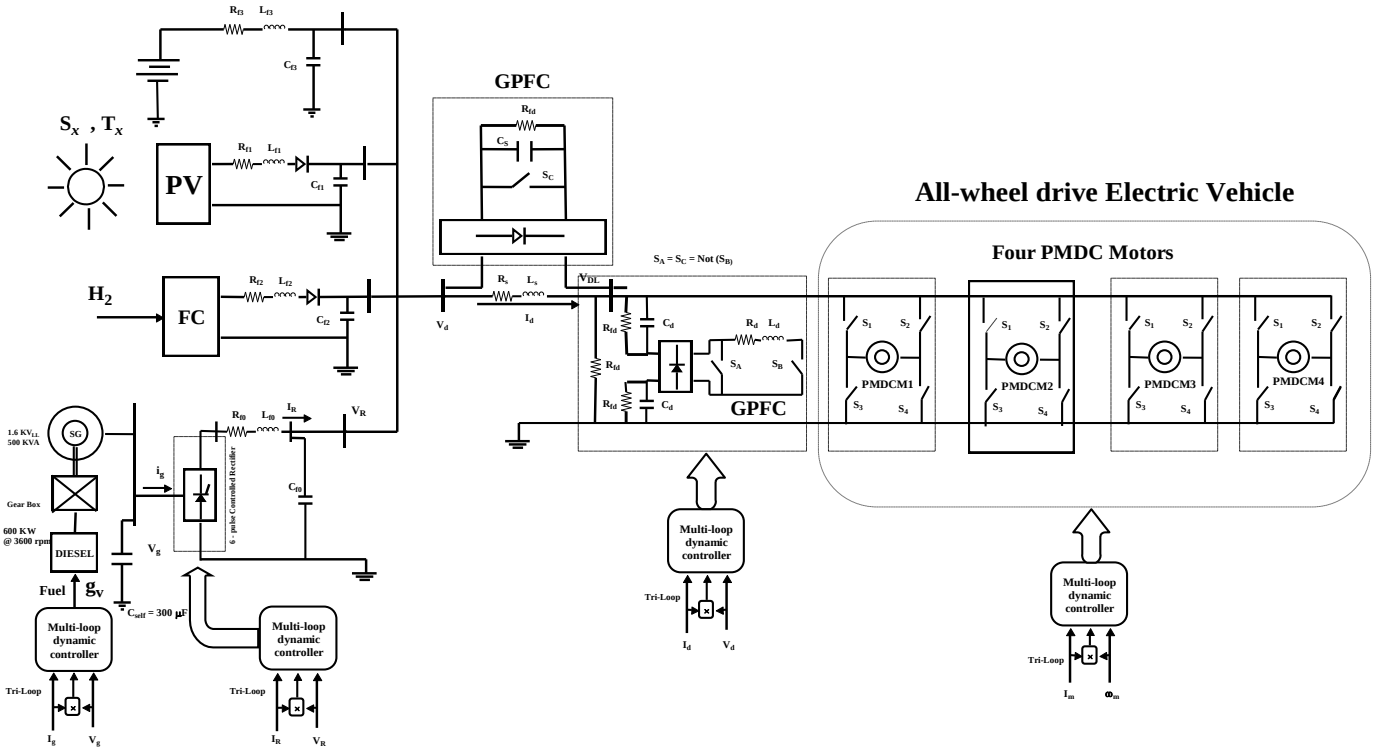

Fig. 4. The hybrid four-wheel EV drive system with PV-FC-Diesel-Battery AC/DC Generation

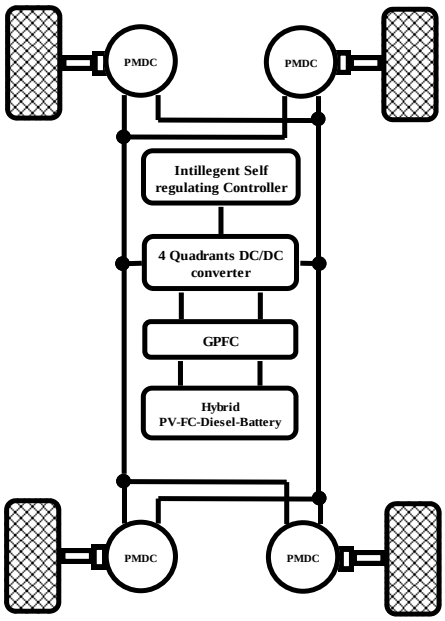

Fig. 5. Schematic diagram of a prototype four-wheel drive electric vehicle using four PMDC motors

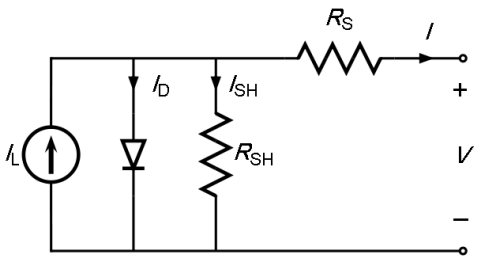

Fig. 6. the equivalent circuit of a solar cell

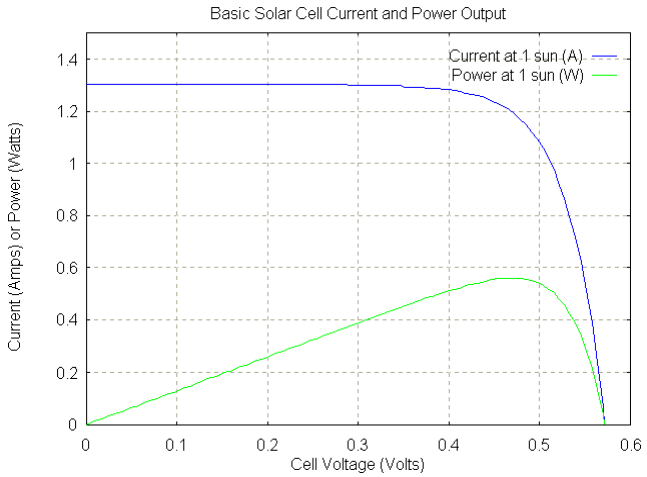

Fig. 7. The dynamic behavior of a solar cell at particular intensities of solar radiation

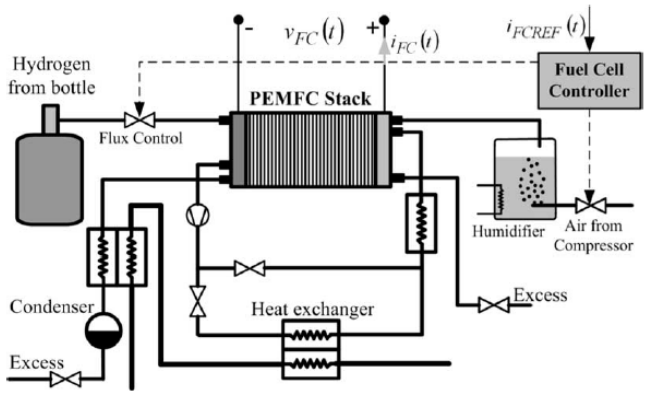

Fig. 8. Simplified diagram of the Fuel Cell PEMF-C system.

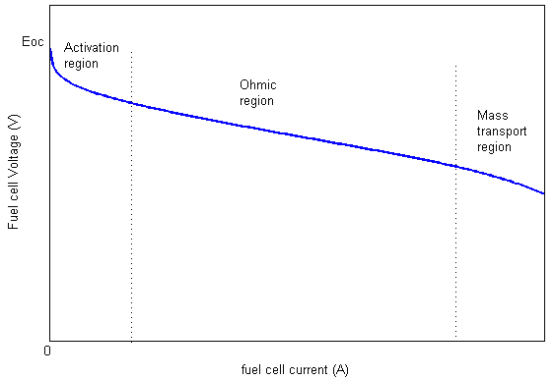

Fig. 9. (V - I) polarization curve of an SOFC

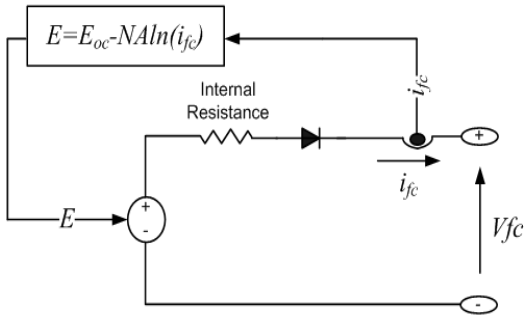

Fig. 10. The equivalent circuit of an electrochemical fuel cell.

Appendix

Synchronous Generator
3 phase, 2 pairs of poles, V_g=0.6 kV (L-L), Sg=3000 KVA, R_s = 0.0036 PU, H = 2, F = 0, P = 2, X_d = 1.56 PU, X_d` = 0.296 PU, X_d`` = 0.177 PU, $X_q$ = 1.06 PU, $X_q$`` = 0.177 PU, X_l = 0.052 PU.
Diesel: 100 KW @ 3600rpm, 240 V, R_{f0} = 0.05 Ohms, L_{f0} = 5 mH, C_{f0} =9000 µF,
Fuel Cell: 100 KW, 240 V_{dc} , R_{f2} = 0.1 Ω, L_{f2} = 10 mH, C_{f2} =9000 µF,Open circuit voltage (V) = 240, nominal voltage = 220 v, maximum voltage = 220 v , nominal power 50 KW , maximum power 110 KW, Nominal current = 227.27A , maximum current 500A Number of Cells = 220 , nominal Efficiency, 55%, Nominal air flow = 1300 lpm, operating temperature = 65 Celsius, Nominal fuel pressure 1.5 bar , nominal air pressure = 1 bar.
PV: 240V, 100 KW, R_{f1} = 0.1 Ω, L_{f1} = 10 mH, C_{f1} =9000 µF, Nom. Voltage 300V, Nominal current 11A, Nom. Power 3300 W, Ns = 100 , Np = 135 , Tx = 20 , Sx = 102.0507, Ipv = 5 , Tc = 20 , Sc = 205 ,
Battery: Nominal voltage: 240 V_{DC}, Rated capacity: 1200 Ah, Initial State-Of-Charge: 100%, Discharge current: 10, 5 A, R_{f3} = 0.1 Ω, L_{f3} = 10 mH, C_{f3} =9000 µF,
DC side GPFC: R_s = 0.1 Ω, L_s = 10 mH, C_s =1775 µF, R_d = 0.2 Ω, L_d = 10 mH, C_d = 6000 µF, R_{fd} = 20 KΩ,
EV-PMDC motor. The armature coil of the DC motor can be presented by an inductance (L_m) in series with resistance (R_m) in series with an induced voltage (e_m) which opposes the voltage source. The differential equations into state space form for the armature current and angular velocity can be written as:

$$\frac{d}{dt}\begin{bmatrix}\omega_r\\ i_a\end{bmatrix}=\begin{bmatrix}-\frac{B}{J} & \frac{K}{J}\\ -\frac{K}{L_a} & -\frac{R}{L_a}\end{bmatrix}\begin{bmatrix}\omega_r\\ i_a\end{bmatrix}+\begin{bmatrix}0\\ \frac{1}{L_a}\end{bmatrix}V_a \quad \omega_r = \begin{bmatrix}1 & 0\end{bmatrix}\begin{bmatrix}\omega_r\\ i_a\end{bmatrix}$$

The load torque is given by and the nonlinear inertia J and viscous friction B have the following variable non-linear forms:

$$T_L = T_0 + T_1\omega_m + T_2\omega_m^2,\ B_m = B_0 + B_1\omega_m + B_2\omega_m^2,\ J_m = J_0 + J_1\omega_m + J_2\omega_m^2$$

where: R_m = 0.1 Ω, L_m = 10 mH, 100 KW, 220 V_{dc}, J_m = 0.7, B_m = 0.08, 3600 rpm , K_e = K_t = 1.06 , T0=1.2, T1=0.006, T2=6.6*10^{-5}, B0=5.8*10^{-3}, B1=25*10^{-6}, B2=0.423*10^{-6}, J0=14.4*10^{-3}, J1=62.6*10^{-6}, J2=1.06*10^{-6}
Control Weightings Scaling: γ_{vd} = 0.86, γ_{Id} = 0.45, γ_{Pd} = 0.25, γ_{vg} = 0.8, γ_{Ig} = 0.50, γ_{Pg} = 0.30, γ_{vR} = 0.75, γ_{IR} = 0.62, γ_{PR} = 0.15, γ_{vm} = 0.92, γ_{Im} = 0.54, γ_{Pm} = 0.24,
Tuned conventional PID controller Gains: 10 $\leq K_{Pg}$,K_{Pd} , K_{PR} , $K_{Pm} \leq 200$, 1 $\leq K_{Ig}$, K_{Id} , K_{IR} , $K_{Im} \leq 20$, 0.1 $\leq K_{Dg}$,K_{Dd} , K_{DR} , $K_{Dm} \leq 10$,
Tuned modified PID controller- I Gains: 50 $\leq$ *KPg ,KPd* , K_{PR} , $K_{Pm} \leq 300$, 1 $\leq K_{Ig}$, K_{Id} , K_{IR} , $K_{Im} \leq 10$, 0.1 $\leq K_{Dg}$,K_{Dd} , K_{DR} , $K_{Dm} \leq 5$, 1 $\leq K_{eg}$,K_{ed} , K_{eR} , $K_{em} \leq 50$,
Tuned modified PID controller – II Gains: 50 $\leq K_{Pg}$,K_{Pd} , K_{PR} , $K_{Pm} \leq 300$, 1 $\leq K_{Ig}$, K_{Id} , K_{IR} , $K_{Im} \leq 10$, 0.1 $\leq K_{Dg}$,K_{Dd} , K_{DR} , $K_{Dm} \leq 5$, 1 $\leq K_{eg}$,K_{ed} , K_{eR} , $K_{em} \leq 100$,
Tuned Variable structure sliding mode controller VSC/SMC/B-B Gains: 1 $\leq \beta_{0g}$, β_{0d} , β_{0R} , $\beta_{0m} \leq 10$, 1 $\leq \beta_{1g}$, β_{1d} , β_{1R} , $\beta_{1m} \leq 50$, 0.01 $\leq K_{\alpha g}$, $K_{\alpha d}$, $K_{\alpha R}$, $K_{\alpha m} \leq 1$

References

[1] Billinton, R.; Yi Gao "Multistate Wind Energy Conversion System Models for Adequacy Assessment of Generating Systems Incorporating Wind Energy" IEEE Transaction on Energy Conversion, Volume 23, Issue 1, March 2008 Page(s):163 - 170

[2] Weihao Hu; Yue Wang; Weizheng Yao; Jinlong Wu; Hailong Zhang; Zhaoan Wang "An efficient experimental method for high power direct drive wind energy conversion systems" Power Electronics Specialists Conference, 2008. PESC 2008. IEEE, 15-19 June 2008 Page(s):3955 – 3959

[3] Pera, M.C.; Hissel, D.; Kauffmann, J.M. "Fuel cell systems for electrical vehicles" Vehicular Technology Conference, 2002, VTC Spring 2002, IEEE 55th, Volume: 4 Page(s): 2097 – 2102.

[4] Parspour, N.; " Novel drive for use in electrical vehicles", Vehicular Technology Conference, 2005. VTC 2005-Spring. 2005 IEEE, 1st , Volume: 5 , Page(s): 2930 - 2933 Vol. 5

[5] Sharaf, A.M.; Ozkop, E.; Altas, I.H. "A Hybrid Photovoltaic PV Array-Battery Powered EV-PMDC Drive Scheme ", Electrical Power Conference, 2007. EPC 2007. IEEE Canada , Page(s): 37 – 43

[6] Zhu, Z.Q.; Chan, C.C.; "Electrical machine topologies and technologies for electric, hybrid, and fuel cell vehicles" Vehicle Power and Propulsion Conference, 2008. VPPC '08. IEEE, Page(s): 1 – 6

[7] Vas, J.V.; Venugopal, S.; Nair, V.G.; "Control scheme for electrical drive of solar powered vehicles" India Conference, 2008. INDICON 2008. Annual IEEE, Volume: 1 , Page(s): 75 – 80

[8] Zhu, Z.Q.; Howe, D.; "Electrical Machines and Drives for Electric, Hybrid, and Fuel Cell Vehicles" Proceedings of the IEEE, Volume: 95 , Issue: 4 , 2007 , Page(s): 746 – 765

[9] Wenzhong Gao, Chris Mi "Hybrid vehicle design using global optimisation algorithms" 10.1504/IJEHV.2007.014447, Pages: 57 - 70

[10] Morteza Mohebbi, Mohammad Farrokhi "Adaptive neuro control of parallel hybrid electric vehicles" 10.1504/IJEHV.2007.014444, Pages: 3 - 19

[11] L. Davis, "Handbooks of genetic algorithm", New York: Van Nostrand, Reinhold, 1991

[12] J. Kennedy and R. Eberhart, "Particle swarm optimization" Proceedings, IEEE International Conf. on Neural Networks, Vol. 4, pp.1942–1948, 1995

[13] Y. Shi and R. Eberhart, "Empirical study of particle swarm optimization" Proceedings of the 1999 Congress on Evolutionary Computation, Vol. 3, 1999.

[14] R. Eberhart and Y Shi, (2001) "Particle swarm optimization: developments, applications and resources" Proceedings of the 2001 Congress on Evolutionary Computation, Vol. 1, pp. 81 -86, 2001.

[15] Y. Shi and R. Eberhart, (1998) "Parameter Selection in Particle Swarm Optimization" Proc. Seventh Annual Conf. on Evolutionary Programming, pp. 591-601, 1998.

[16] Ngatchou, P.; Zarei, A.; El-Sharkawi, A.; (2005) "Pareto Multi Objective Optimization" Intelligent Systems Application to Power Systems, 2005. Proceedings of the 13th International Conference on 6-10 Nov. 2005 Page(s):84 – 91

[17] Berizzi, A., M. Innorta, and P. Marannino. (2001) "Multiobjective optimization techniques applied to modern power systems". In 2001 IEEE Power Engineering Society Winter Meeting, Jan 28-Feb 1 2001.

[18] C. A. Coello Coello and M. S. Lechuga. (2003) "MOPSO: A proposal for multiple objective particle swarm optimization". In IEEE Proceedings World Congress on Computational Intelligence, pages 1051–1056, 2003.

[19] K. Deb, A. Paratap, S. Agarwal, and T. Meyarivan, "A Fast and Elitist Multi-objective Genetic Algorithm: NSGA-II," IEEE Trans. Evolutionary Computation, no. 2, pp. 182-197, 2002.

[20] N. Srinivas and K. Deb, "Multiobjective optimization using nondominated sorting in genetic algorithms," Tech. Rep., Dept. Mechanical Engineering, Kanput, India, 1993.

[21] Antonio Luque and Steven Hegedus (2003), "Handbook of Photovoltaic Science and Engineering", John Wiley and Sons, ISBN 0471491969.

[22] Jenny Nelson (2003). "The Physics of Solar Cells". Imperial College Press. ISBN 978-1-86094-340-9.

[23] Thounthong, P.; Rael, S.; Davat, B.; 2009 "Analysis of Supercapacitor as Second Source Based on Fuel Cell Power Generation" Energy conversion, ieee transactions , Volume 24, Issue 1, March 2009 Page(s):247 - 255

[24] Gebregergis, A.; Pillay, P.; Bhattacharyya, D.; Rengaswemy, R.; 2009 "Solid Oxide Fuel Cell Modeling" Industrial Electronics, IEEE Transactions, Volume 56, Issue 1, Jan. 2009 Page(s):139 - 148

[25] Ismail H. Altas, Emre Oz kop and Adel M. Sharaf, "A Novel PV-Powered Standalone Village Electricity Utilization Fuzzy Logic Dynamic Controller Strategy", INISTA 2009, International Symposium on INnovations in Intelligent SysTems and Applications, June 29-July 1, 2009, TRABZON, TURKEY.

Table 1. DC bus dynamic behavior comparison using the constant parameters conventional PID controller

	The First Speed Track	The Second Speed Track	The Third Speed Track
DC bus voltage (PU)	0.85274	0.8819	0.8618
DC bus current (PU)	0.72463	0.74817	0.7706
Maximum Transient DC Voltage Over/Under Shoot (PU)	0.07353	0.07030	0.06916
Maximum Transient DC Current – Over/Under Shoot (PU)	0.08681	0.09954	0.08890
DC System Efficiency	0.88027	0.873267	0.89690
NMSE_$V_{DC\text{-}bus}$	0.07544	0.06263	0.06575
NMSE_ω_m	0.08000	0.07681	0.07176
PMDCM total controller Error e_{tm}	0.06760	0.05513	0.05150
DC side GPFC Error e_{td}	0.06204	0.0812	0.08045
The diesel engine gen set total controller Error e_{tg}	0.04719	0.04959	0.04890
The diesel engine converter total controller Error e_{tR}	0.05119	0.04249	0.05236

Table 2. DC bus dynamic behavior comparison using the constant parameters modified PID controller- I

	The First Speed Track	The Second Speed Track	The Third Speed Track
DC bus voltage (PU)	0.905384	0.903496	0.892775
DC bus current (PU)	0.72200	0.71977	0.719416
Maximum Transient DC Voltage Over/Under Shoot (PU)	0.06112	0.062632	0.06590
Maximum Transient DC Current – Over/Under Shoot (PU)	0.0986	0.085243	0.082528
DC System Efficiency	0.890201	0.891517	0.88194
NMSE_$V_{DC\text{-}bus}$	0.09717	0.08323	0.08091
NMSE_ω_m	0.06013	0.05022	0.0478
PMDCM total controller Error e_{tm}	0.07613	0.08924	0.09714
DC side GPFC Error e_{td}	0.08899	0.07240	0.074800
The diesel engine gen set total controller Error e_{tg}	0.06355	0.064996	0.065998
The diesel engine converter total controller Error e_{tR}	0.051087	0.053814	0.055153

Table 3. DC bus dynamic behavior comparison using the constant parameters modified PID controller – II

	The First Speed Track	The Second Speed Track	The Third Speed Track
DC bus voltage (PU)	0.89615	0.91325	0.904000
DC bus current (PU)	0.72549	0.74441	0.74225
Maximum Transient DC Voltage Over/Under Shoot (PU)	0.06624	0.0655	0.05790
Maximum Transient DC Current – Over/Under Shoot (PU)	0.08577	0.09802	0.08502
DC System Efficiency	0.904078	0.916877	0.897981
NMSE_$V_{DC\text{-}bus}$	0.051532	0.06109	0.059779
NMSE_ω_m	0.05488	0.06130	0.07716
PMDCM total controller Error e_{tm}	0.07479	0.08187	0.08401
DC side GPFC Error e_{td}	0.0567	0.06634	0.06550
The diesel engine gen set total controller Error e_{tg}	0.05402	0.054390	0.052790
The diesel engine converter total controller Error e_{tR}	0.044016	0.04346	0.042488

Table 4. DC bus dynamic behavior comparison using the constant parameters Variable structure sliding mode controller VSC/SMC/B-B

	The First Speed Track	The Second Speed Track	The Third Speed Track
DC bus voltage (PU)	0.904060	0.917020	0.895291
DC bus current (PU)	0.76545	0.769594	0.769731
Maximum Transient DC Voltage Over/Under Shoot (PU)	0.052925	0.054604	0.053089
Maximum Transient DC Current – Over/Under Shoot (PU)	0.09461	0.087336	0.081906
DC System Efficiency	0.885737	0.906631	0.895666
NMSE_$V_{DC\text{-}bus}$	0.09512	0.08443	0.084672
NMSE_ω_m	0.05131	0.053548	0.053953
PMDCM total controller Error e_{tm}	0.08521	0.095145	0.09422
DC side GPFC Error e_{td}	0.072338	0.70746	0.703462
The diesel engine gen set total controller Error e_{tg}	0.062513	0.067513	0.069606
The diesel engine converter total controller Error e_{tR}	0.08856	0.086233	0.085740

Table 5. DC bus dynamic behavior comparison using ANN Controller

	The First Speed Track	The Second Speed Track	The Third Speed Track
DC bus voltage (PU)	0.92747	0.932736	0.91131
DC bus current (PU)	0.661466	0.67464	0.64627
Maximum Transient DC Voltage Over/Under Shoot (PU)	0.0372	0.04186	0.05541
Maximum Transient DC Current – Over/Under Shoot (PU)	0.08575	0.07355	0.06083
DC System Efficiency	0.916100	0.928253	0.926261
NMSE_$V_{DC\text{-}bus}$	0.03439	0.04827	0.05231
NMSE_ω_m	0.03793	0.02627	0.03146
PMDCM total controller Error e_{tm}	0.04261	0.04200	0.04639
DC side GPFC Error e_{td}	0.02397	0.02416	0.02440
The diesel engine gen set total controller Error e_{tg}	0.04437	0.04507	0.05522
The diesel engine converter total controller Error e_{tR}	0.03388	0.03978	0.03463

Table 6. DC bus dynamic behavior comparison using FLC Controller

	The First Speed Track	The Second Speed Track	The Third Speed Track
DC bus voltage (PU)	0.943860	0.94745	0.930581
DC bus current (PU)	0.65611	0.64712	0.630216
Maximum Transient DC Voltage Over/Under Shoot (PU)	0.03898	0.03126	0.02065
Maximum Transient DC Current – Over/Under Shoot (PU)	0.05658	0.04383	0.05014
DC System Efficiency	0.926459	0.92890	0.937334
NMSE_$V_{DC\text{-}bus}$	0.04193	0.03022	0.02129
NMSE_ω_m	0.0192	0.02016	0.02024
PMDCM total controller Error e_{tm}	0.02956	0.02154	0.02852
DC side GPFC Error e_{td}	0.06562	0.09179	0.07781
The diesel engine gen set total controller Error e_{tg}	0.0337	0.02964	0.02928
The diesel engine converter total controller Error e_{tR}	0.02533	0.0260	0.02051

Table 7. DC bus dynamic behavior comparison using the GA based Tuned conventional PID controller

	The First Speed Track	The Second Speed Track	The Third Speed Track
DC bus voltage (PU)	0.96034	0.96062	0.95384
DC bus current (PU)	0.55232	0.530199	0.52200
Maximum Transient DC Voltage Over/Under Shoot (PU)	0.00463	0.004936	0.004112
Maximum Transient DC Current – Over/Under Shoot (PU)	0.00625	0.006094	0.00686
DC System Efficiency	0.95008	0.94777	0.940201
NMSE_$V_{DC\text{-}bus}$	0.008980	0.007076	0.009717
NMSE_ω_m	0.00890	0.008819	0.008013
PMDCM total controller Error e_{tm}	0.007843	0.008708	0.007613
DC side GPFC Error e_{td}	0.00808	0.009078	0.008899
The diesel engine gen set total controller Error e_{tg}	0.003159	0.003974	0.003355
The diesel engine converter total controller Error e_{tR}	0.005447	0.006566	0.005087

Table 8. DC bus dynamic behavior comparison using the PSO based Tuned conventional PID controller

	The First Speed Track	The Second Speed Track	The Third Speed Track
DC bus voltage (PU)	0.9669	0.97230	0.97563
DC bus current (PU)	0.514	0.5425	0.53732
Maximum Transient DC Voltage Over/Under Shoot (PU)	0.003996	0.003582	0.003519
Maximum Transient DC Current – Over/Under Shoot (PU)	0.005818	0.005555	0.005554
DC System Efficiency	0.9514	0.9582	0.9545
NMSE_$V_{DC\text{-}bus}$	0.006834	0.006009	0.006485
NMSE_ω_m	0.007303	0.007419	0.007647
PMDCM total controller Error e_{tm}	0.007809	0.007945	0.007844
DC side GPFC Error e_{td}	0.008160	0.008953	0.008946
The diesel engine gen set total controller Error e_{tg}	0.002584	0.002487	0.002268
The diesel engine converter total controller Error e_{tR}	0.005116	0.005391	0.004967

Table 9. DC bus dynamic behavior comparison using the GA based Tuned modified PID controller- I

	The First Speed Track	The Second Speed Track	The Third Speed Track
DC bus voltage (PU)	0.96187	0.9861	0.9688
DC bus current (PU)	0.63637	0.62814	0.64958
Maximum Transient DC Voltage Over/Under Shoot (PU)	0.009881	0.009151	0.008854
Maximum Transient DC Current – Over/Under Shoot (PU)	0.007214	0.008397	0.007821
DC System Efficiency	0.941726	0.933797	0.9428082
NMSE_$V_{DC\text{-}bus}$	0.008879	0.009372	0.00827
NMSE_ω_m	0.005380	0.007118	0.006406
PMDCM total controller Error e_{tm}	0.005219	0.007699	0.006228
DC side GPFC Error e_{td}	0.006572	0.006135	0.00507
The diesel engine gen set total controller Error e_{tg}	0.009807	0.006440	0.007512
The diesel engine converter total controller Error e_{tR}	0.003507	0.007476	0.003144

Table 10. DC bus dynamic behavior comparison using the PSO based Tuned modified PID controller- I

0	The First Speed Track	The Second Speed Track	The Third Speed Track
DC bus voltage (PU)	0.97079	0.97350	0.96469
DC bus current (PU)	0.60940	0.61669	0.6103
Maximum Transient DC Voltage Over/Under Shoot (PU)	0.008343	0.007736	0.009398
Maximum Transient DC Current – Over/Under Shoot (PU)	0.007109	0.007235	0.006118
DC System Efficiency	0.9581	0.95622	0.95755
NMSE_$V_{DC\text{-}bus}$	0.008598	0.007157	0.009750
NMSE_ω_m	0.007527	0.006477	0.007515
PMDCM total controller Error e_{tm}	0.006636	0.005898	0.004823
DC side GPFC Error e_{td}	0.008887	0.004256	0.009305
The diesel engine gen set total controller Error e_{tg}	0.008107	0.007857	0.003648
The diesel engine converter total controller Error e_{tR}	0.008215	0.007545	0.00974

Table 11. DC bus dynamic behavior comparison using the GA based Tuned modified PID controller – II

	The First Speed Track	The Second Speed Track	The Third Speed Track
DC bus voltage (PU)	0.95337	0.96469	0.96299
DC bus current (PU)	0.6243	0.61953	0.624408
Maximum Transient DC Voltage Over/Under Shoot (PU)	0.006114	0.0054632	0.0054971
Maximum Transient DC Current – Over/Under Shoot (PU)	0.008818	0.008899	0.007111
DC System Efficiency	0.93278	0.94371	0.95523
NMSE_$V_{DC\text{-}bus}$	0.004069	0.005516	0.004373
NMSE_ω_m	0.006497	0.006859	0.005911
PMDCM total controller Error e_{tm}	0.001145	0.0013194	0.001645
DC side GPFC Error e_{td}	0.005925	0.0052439	0.0059193
The diesel engine gen set total controller Error e_{tg}	0.004696	0.004942	0.0041476
The diesel engine converter total controller Error e_{tR}	0.007099	0.0066789	0.0069821

Table 12. DC bus dynamic behavior comparison using the PSO based Tuned modified PID controller – II

	The First Speed Track	The Second Speed Track	The Third Speed Track
DC bus voltage (PU)	0.96841	0.964346	0.964428
DC bus current (PU)	0.619458	0.618023	0.618519
Maximum Transient DC Voltage Over/Under Shoot (PU)	0.007662	0.009669	0.007012
Maximum Transient DC Current – Over/Under Shoot (PU)	0.00754164	0.00753175	0.00759818
DC System Efficiency	0.943307	0.953824	0.948052
NMSE_$V_{DC\text{-}bus}$	0.005423	0.006396	0.006727
NMSE_ω_m	0.005123	0.0054443	0.0057547
PMDCM total controller Error e_{tm}	0.0016667	0.0015124	0.0018915
DC side GPFC Error e_{td}	0.0063503	0.0064763	0.0065155
The diesel engine gen set total controller Error e_{tg}	0.0054647	0.005347	0.0052206
The diesel engine converter total controller Error e_{tR}	0.0073583	0.0074459	0.008394

Table 13. DC bus dynamic behavior comparison using the GA based Tuned Variable structure sliding mode controller VSC/SMC/B-B

	The First Speed Track	The Second Speed Track	The Third Speed Track
DC bus voltage (PU)	0.964652	0.97417	0.964182
DC bus current (PU)	0.60878	0.614695	0.613914
Maximum Transient DC Voltage Over/Under Shoot (PU)	0.0085931	0.009302	0.008437
Maximum Transient DC Current – Over/Under Shoot (PU)	0.002005	0.00292	0.0028122
DC System Efficiency	0.9404	0.948156	0.94302
NMSE_$V_{DC\text{-}bus}$	0.0073133	0.007304	0.008248
NMSE_ω_m	0.0074627	0.0076308	0.008558
PMDCM total controller Error e_{tm}	0.008187	0.009167	0.007663
DC side GPFC Error e_{td}	0.003062	0.004618	0.004337
The diesel engine gen set total controller Error e_{tg}	0.0047025	0.005121	0.004377
The diesel engine converter total controller Error e_{tR}	0.002879	0.003265	0.002328

Table 14. DC bus dynamic behavior comparison using the PSO based Tuned Variable structure sliding mode controller VSC/SMC/B-B

	The First Speed Track	The Second Speed Track	The Third Speed Track
DC bus voltage (PU)	0.97347	0.974602	0.950341
DC bus current (PU)	0.604077	0.607674	0.605076
Maximum Transient DC Voltage Over/Under Shoot (PU)	0.0073109	0.007259	0.008571
Maximum Transient DC Current – Over/Under Shoot (PU)	0.004746	0.005987	0.0047885
DC System Efficiency	0.932558	0.930708	0.9327892
NMSE_$V_{DC\text{-}bus}$	0.004941	0.005854	0.0052055
NMSE_ω_m	0.0065287	0.006309	0.007071
PMDCM total controller Error e_{tm}	0.005095	0.0048638	0.0052238
DC side GPFC Error e_{td}	0.0072358	0.0074294	0.007769
The diesel engine gen set total controller Error e_{tg}	0.0069206	0.007013	0.0071823
The diesel engine converter total controller Error e_{tR}	0.005167	0.0053836	0.0052152

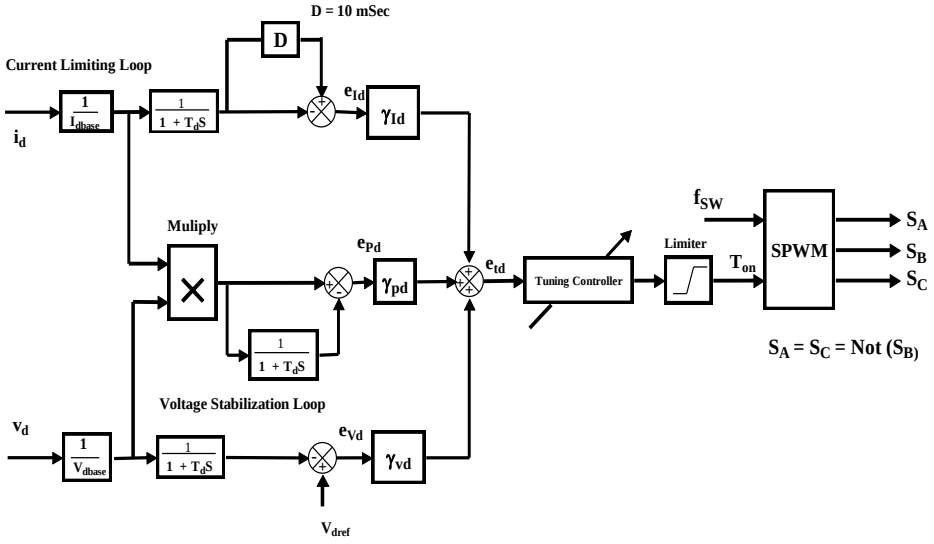

Fig. 11. Tri-loop error driven self regulating self adjusting dynamic controller for the common DC side - GPFC Scheme

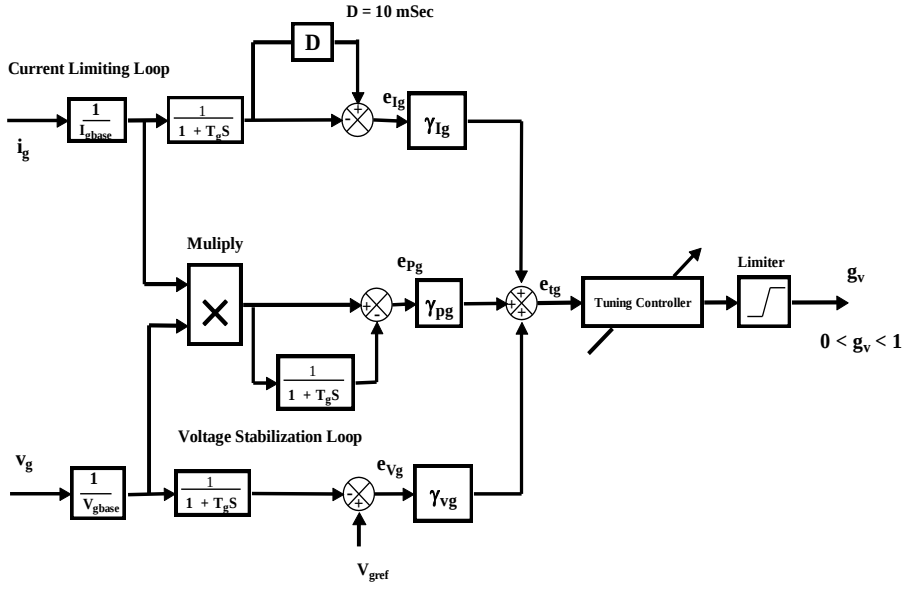

Fig. 12. Tri-loop error driven self regulating self adjusting dynamic controller for the diesel engine generator set

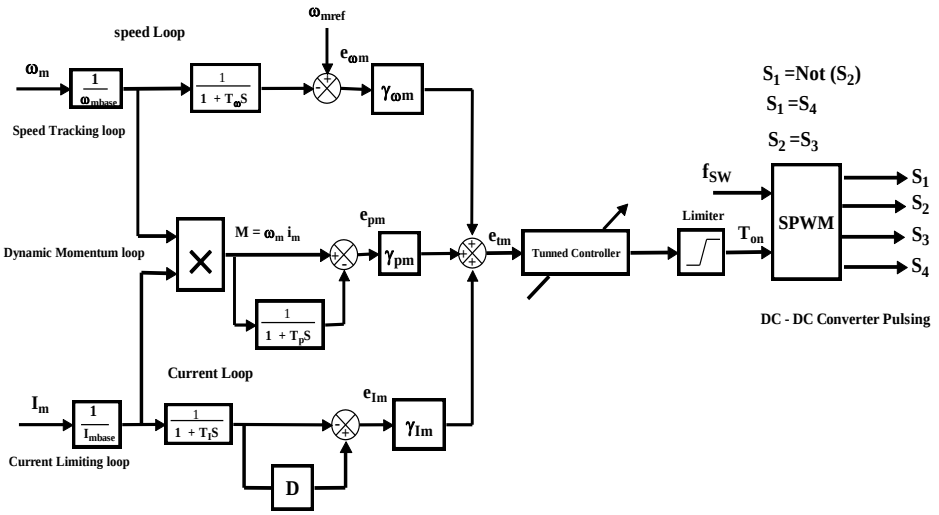

Fig. 13. Tri-loop error driven self regulating self adjusting dynamic controller for dynamic speed control PMDC motor drive

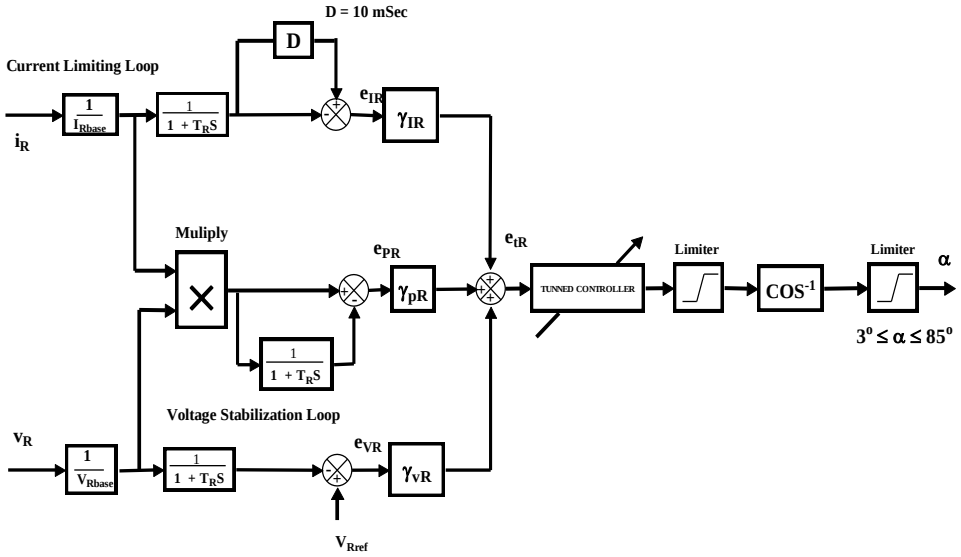

Fig. 14. Tri-loop error driven self regulating self adjusting firing angle α- controller for Diesel AC side rectifier scheme

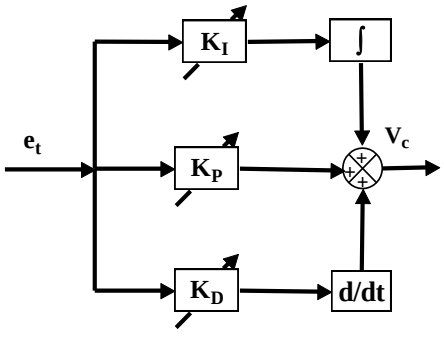

Fig. 15. Conventional self tuned PID controller block diagram.

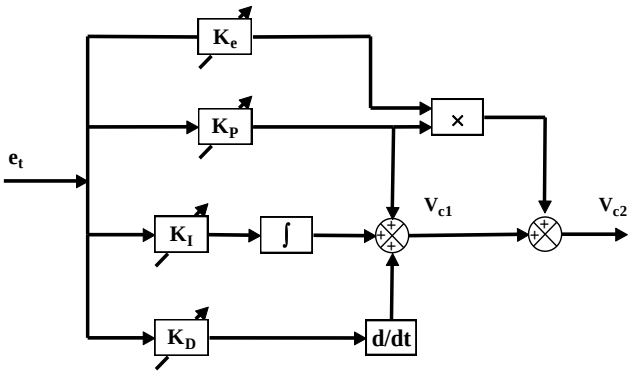

Fig. 16. Weighted modified self tuned PID controller- I block diagram.

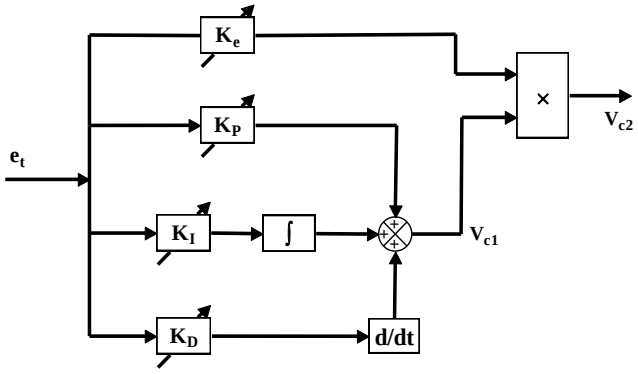

Fig. 17. Weighted modified self tuned PID controller – II block diagram.

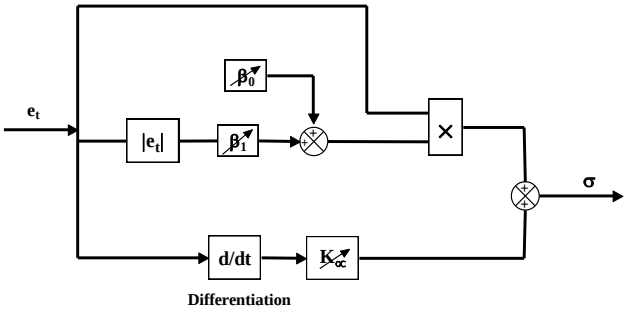

Fig. 18. VSC/SMC self tuned sliding mode controller block diagram.

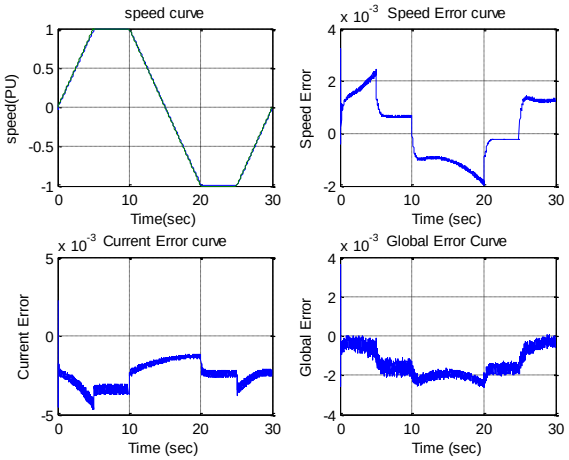

Fig. 19. EV-PMDC Motor Speed response for the first speed track using GA based tuned Tri-loop conventional PID controller

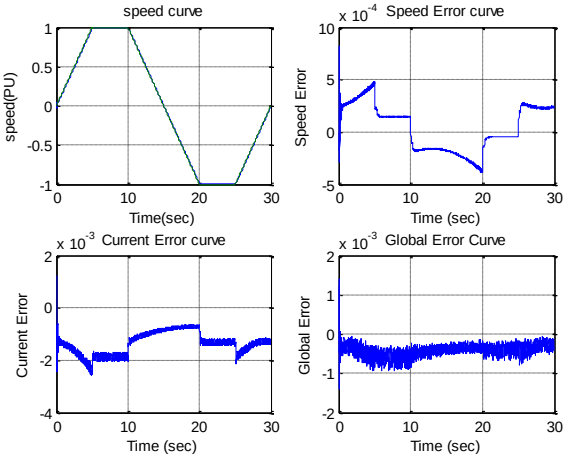

Fig. 20. EV-PMDC Motor Speed response for the first speed track using PSO based tuned Tri-loop conventional PID controller

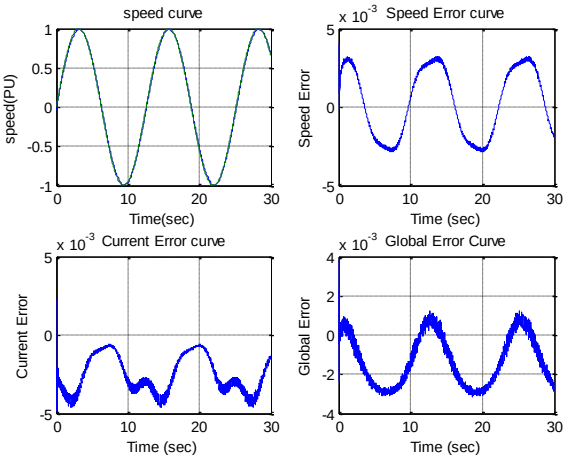

Fig. 21. EV-PMDC Motor Speed response for the Second speed track using GA based tuned Tri-loop conventional PID controller

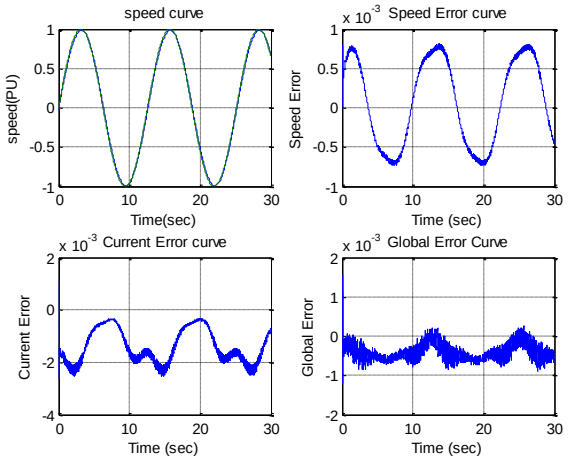

Fig. 22. EV-PMDC Motor Speed response for the Second speed track using PSO based tuned Tri-loop conventional PID controller

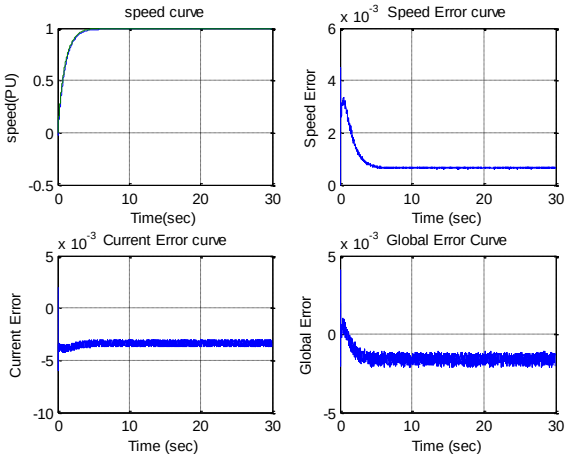

Fig. 23. EV-PMDC Motor Speed response for the third speed track using GA based tuned Tri-loop conventional PID controller

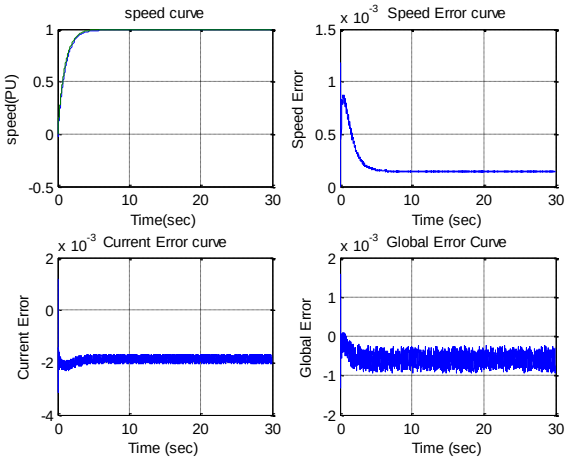

Fig. 24. EV-PMDC Motor Speed response for the third speed track using PSO based tuned Tri-loop conventional PID controller

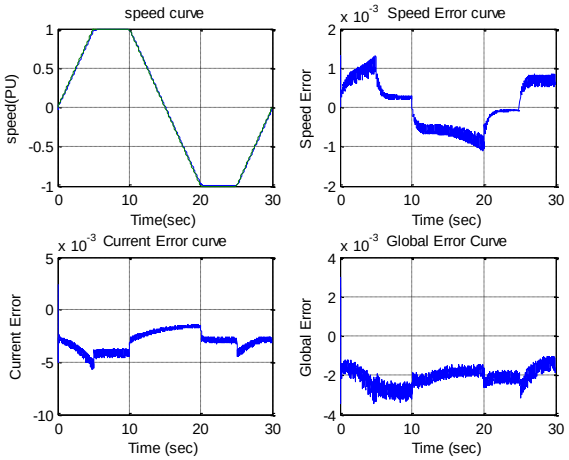

Fig. 25. EV-PMDC Motor Speed response for the first speed track using GA based tuned Tri-loop modified PID controller- I

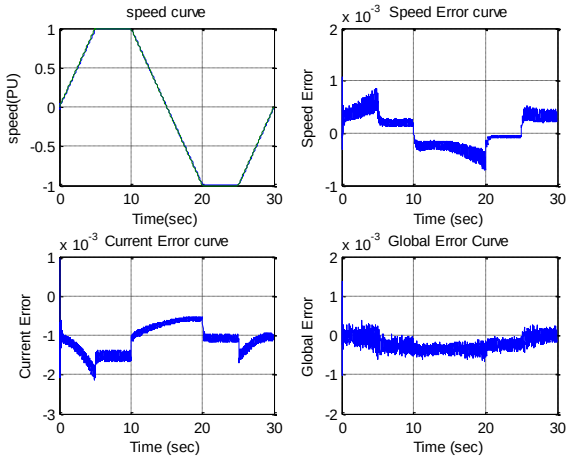

Fig. 26. EV-PMDC Motor Speed response for the first speed track using PSO based tuned Tri-loop modified PID controller- I

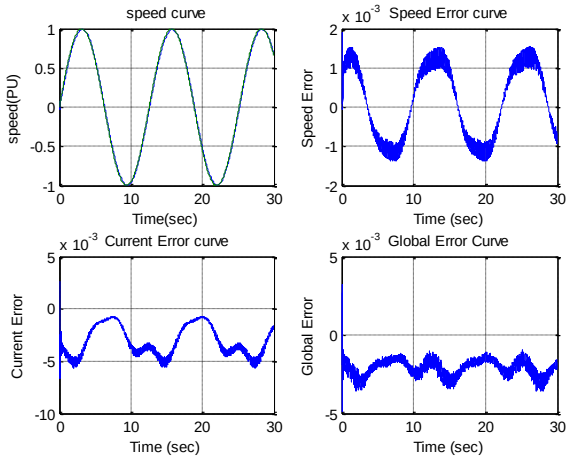

Fig. 27. EV-PMDC Motor Speed response for the Second speed track using GA based tuned Tri-loop modified PID controller- I

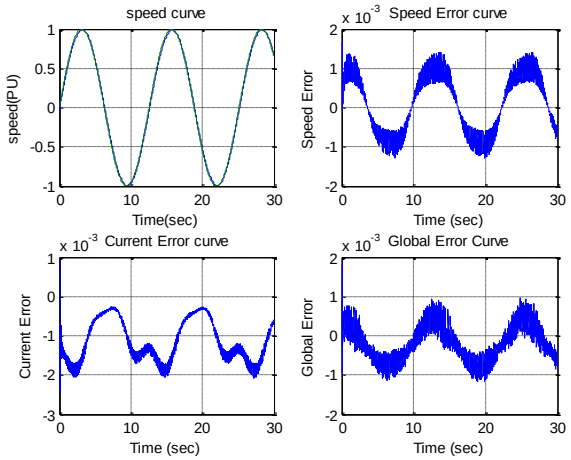

Fig. 28. EV-PMDC Motor Speed response for the Second speed track using PSO based tuned Tri-loop modified PID controller- I

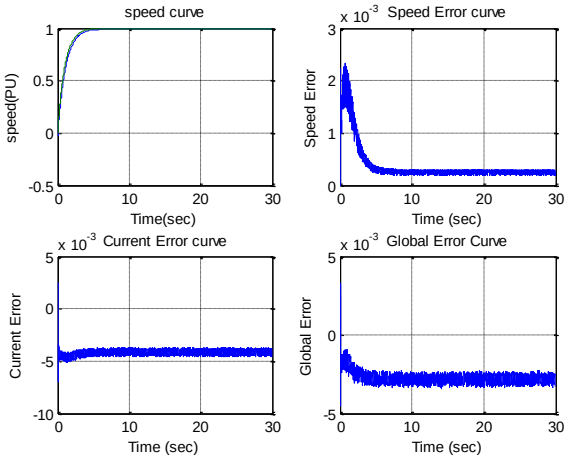

Fig. 29. EV-PMDC Motor Speed response for the third speed track using GA based tuned Tri-loop modified PID controller- I

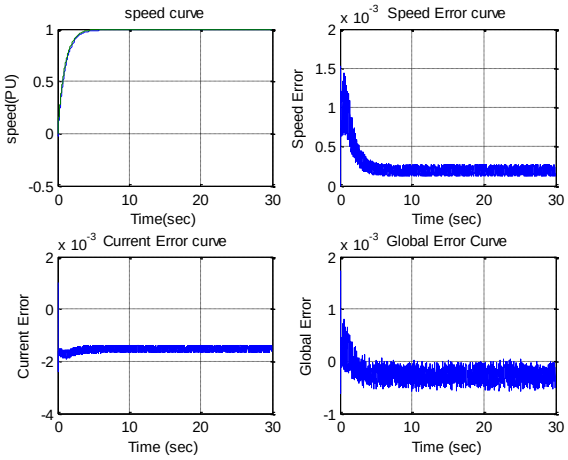

Fig. 30. EV-PMDC Motor Speed response for the third speed track using PSO based tuned Tri-loop modified PID controller- I

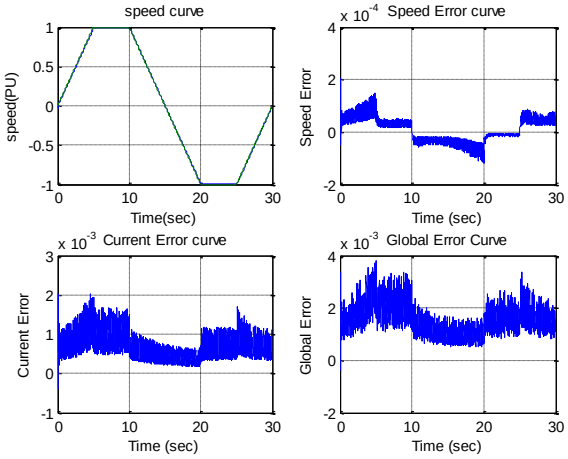

Fig. 31. EV-PMDC Motor Speed response for the first speed track using GA based tuned Tri-loop modified PID controller- II

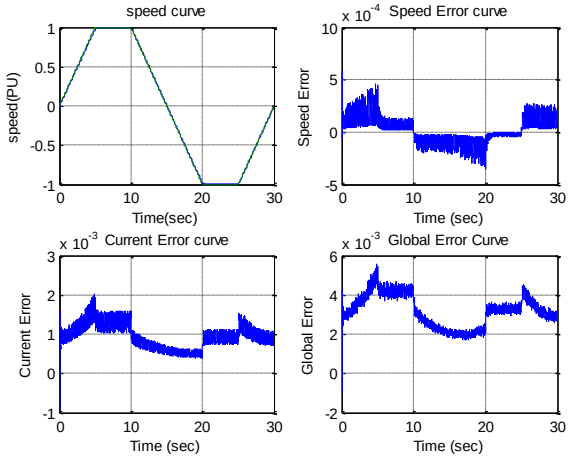

Fig. 32. EV-PMDC Motor Speed response for the first speed track using PSO based tuned Tri-loop modified PID controller- II

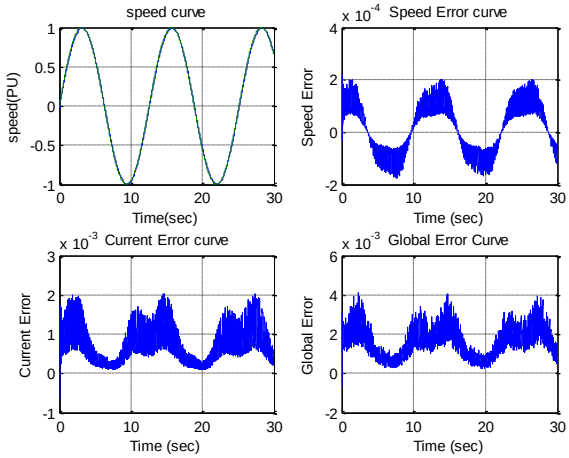

Fig. 33. EV-PMDC Motor Speed response for the Second speed track using GA based tuned Tri-loop modified PID controller- II

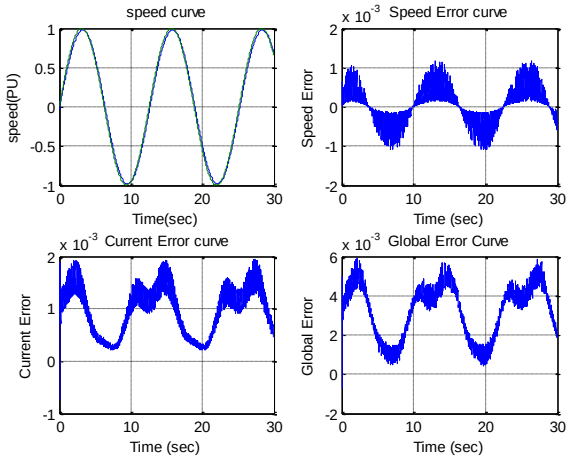

Fig. 34. EV-PMDC Motor Speed response for the Second speed track using PSO based tuned Tri-loop modified PID controller- II

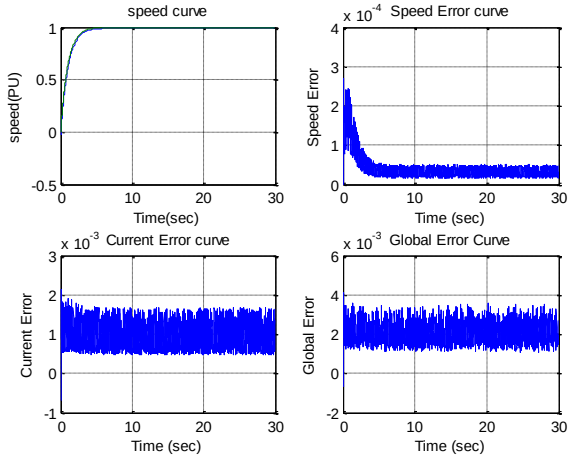

Fig. 35. EV-PMDC Motor Speed response for the third speed track using GA based tuned Tri-loop modified PID controller- II

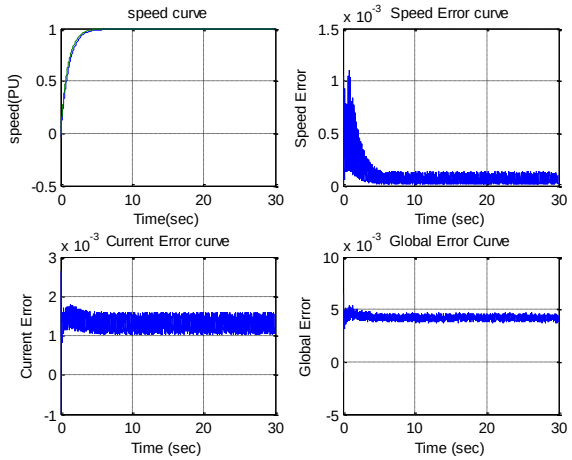

Fig. 36. EV-PMDC Motor Speed response for the third speed track using PSO based tuned Tri-loop modified PID controller- II

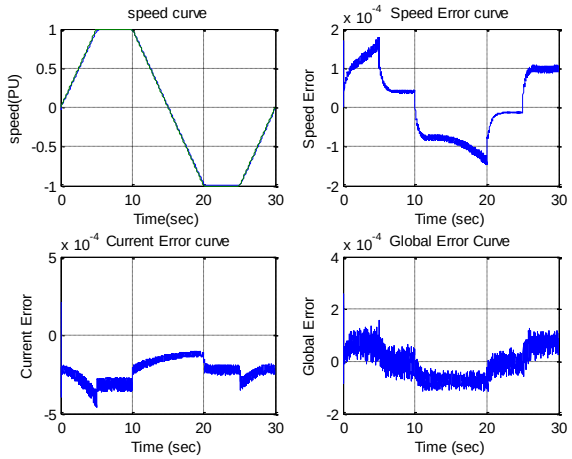

Fig. 37. EV-PMDC Motor Speed response for the first speed track using GA based tuned Tri-loop Variable structure sliding mode controller VSC/SMC/B-B

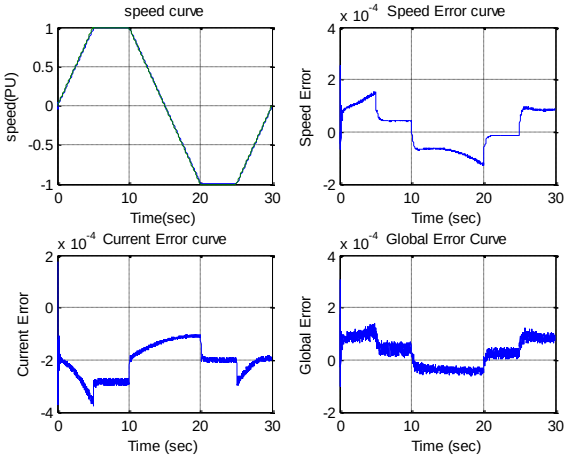

Fig. 38. EV-PMDC Motor Speed response for the first speed track using PSO based tuned Tri-loop Variable structure sliding mode controller VSC/SMC/B-B

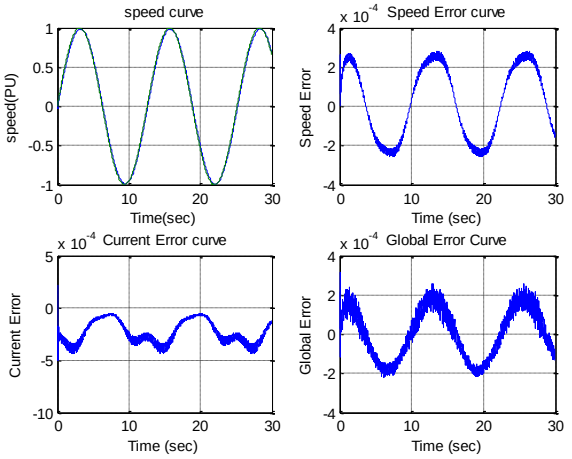

Fig. 39. EV-PMDC Motor Speed response for the Second speed track using GA based tuned Tri-loop Variable structure sliding mode controller VSC/SMC/B-B

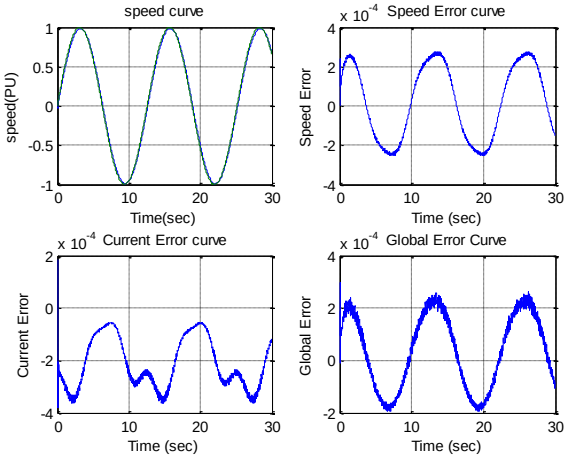

Fig. 40. EV-PMDC Motor Speed response for the Second speed track using PSO based tuned Tri-loop Variable structure sliding mode controller VSC/SMC/B-B

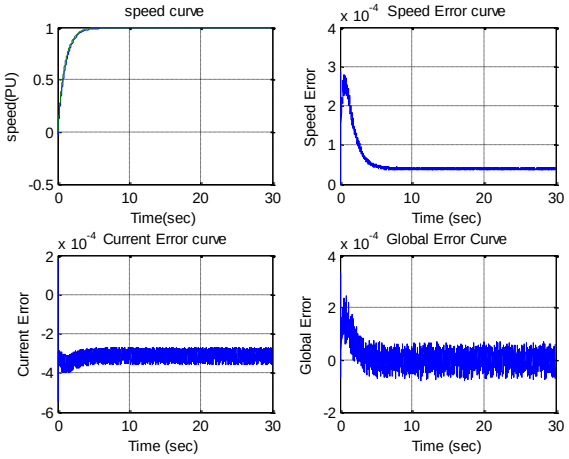

Fig. 41. EV-PMDC Motor Speed response for the third speed track using GA based tuned Tri-loop Variable structure sliding mode controller VSC/SMC/B-B

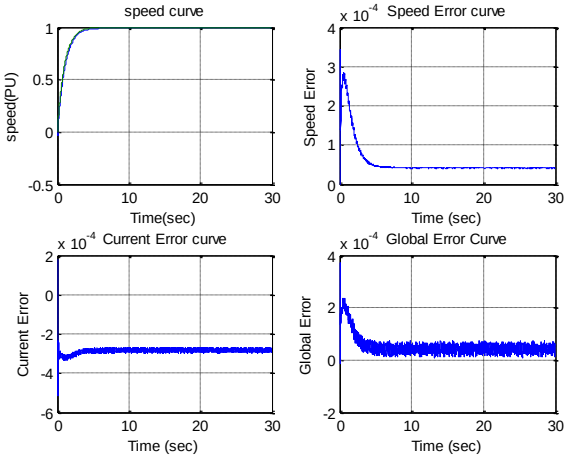

Fig. 42. EV-PMDC Motor Speed response for the third speed track using PSO based tuned Tri-loop Variable structure sliding mode controller VSC/SMC/B-B